# Evaluating the influence of sea surface temperature on tropical cyclone genesis: observations and simulations

Cécile Defforge

Master of Science

Atmospheric and Oceanic Sciences

McGill University

Montreal,Quebec

2016-04-01

Requirements Statement

# DEDICATION

A Valérie.

## ACKNOWLEDGMENTS

I express my deepest gratitude to Timothy Merlis, who has been an amazing supervisor during my Master studies! I really enjoyed our weekly meetings during which his very constructive comments and pieces of advice helped me learn a lot. He has been really helpful, encouraging, and available during all the steps of my Master studies and while co-writing two manuscripts that correspond to chapters 3 and 4. He offered me the great opportunity to submit two papers and to attend the AMS $32^{nd}$ Conference on Hurricanes and Tropical Meteorology, which was more than expected for my Master's. I would like to thank the Atmospheric and Oceanic Department Faculty staff, especially David Straub and Paula, without who I would not have transferred to the AOS department, and Emily who was always here for any administrative questions. I would like to acknowledge the Stephen and Anastasia Mysak Graduate Fellowship for the financial support it provided. My family, and especially my mother, deserves more thanks than I could ever give for their unfailing support and encouragement throughout my graduate studies. I would also render a special thanks to Julia, who is always ready to help me in any way and took the pleasure to visit me in Montreal. Last but not least, I would like to thank all my friends in Montreal and all over the world who listened to my hurricane stories, gave me some brilliant ideas for research, and supported me during these two years.

## ABSTRACT

Tropical cyclones are one of the most dangerous natural disasters and their genesis frequency is tightly linked to environmental conditions. Warm sea surface temperature (SST) is thought to be one of the factors favorable to tropical cyclone (TC) genesis. Recent studies have examined the role of anthropogenic changes in sea surface temperature and other environmental variables in determining changes in tropical cyclone genesis. Here, a basin-by-basin analysis of the SST distributions in the five most active ocean basins shows that the distributions of genesis SST are close to normal distributions that differ between basins, indicating that an apparent global threshold arises from the climatologically coldest basins. Furthermore, the resemblance between these distributions and those of SSTs observed during summer indicates that warm SSTs favor TC genesis only over the cold half of the SSTs encountered during summer, except for the East Pacific basin. In contrast to SST, the distribution of the difference between upper- and lower-level equivalent potential temperature, a measure of convective instability, differs substantially between TC genesis and summer seasons. There is a high level of correlation between time series of SST at TC genesis and SST observed over the main development regions and periods, and both feature significant warming trends over the past 30 years. These time series are also similar to those obtained considering all tropical deep convection events. While the long-term trend in SST observed during tropical deep convection events has previously been documented, the trend in SST at tropical cyclogenesis is a newly detected anthropogenic TC change. The warming trend observed for genesis SST is mostly due to the temporal warming of the oceans, which is slightly counterbalanced by the effect of poleward track migration, toward climatologically colder regions. Last, simulations of zonally asymmetric climate states with different $CO_2$ concentrations show that TC frequency is mostly sensitive to the meridional shift of the inter-tropical convergence zone and, to a smaller extent, to SST changes. The local response of environmental

variables (SST and precipitation rate) and of the TC frequency in the simulated cold region is stronger than in the warm region, resulting in a global decrease in the number of TCs and hurricanes, relative to symmetric climate states.

## RÉSUMÉ

Les cyclones tropicaux sont parmi les catastrophes naturelles les plus dangereuses, et leur formation est étroitement liée aux conditions environnementales. La température élevée des eaux de surface des océans (SST) est considérée comme l'un des facteurs favorisant la formation de cyclones tropicaux (TC). De nombreuses variables environnementales, dont la température de surface des océans, ont été perturbées par les activités humaines au cours des dernières décennies. Des études récentes ont examiné l'impact de ces changements climatiques sur la formation des cyclones tropicaux. Dans la présente étude, l'analyse bassin-par-bassin des températures de surface, dans les cinq bassins océaniques les plus actifs, montre que les distributions des températures au moment de la formation des cyclones sont proches de distributions gaussiennes et diffèrent d'un bassin à l'autre. Ceci indique donc que la définition à l'échelle globale d'un seuil minimum de température nécessaire à la formation de cyclones, est faussée par les bassins climatologiquement les plus froids. Par ailleurs, la comparaison de la distribution des températures au moment de la formation des cyclones avec la distribution des températures observées pendant la saison cyclonique indique qu'augmenter la température de l'eau favorise la formation des cyclones seulement pour les températures les plus froides observées pendant cette saison, sauf pour le Pacifique Est. Contrairement aux températures de surface, la distribution de la différence de température potentielle équivalente entre la haute et la basse troposphère, qui est une mesure de l'instabilité convective, diffère substantiellement entre la formation des cyclones et la saison cyclonique. Il y a une forte corrélation entre les séries temporelles de la température de surface au moment de la formation des cyclones et celles des températures observées pendant les saisons cycloniques dans les régions principales de formation des cyclones, et les deux montrent un réchauffement significatif au cours des 30 dernières années. Ces séries temporelles sont également similaires à celles obtenues en considérant tous les événements de convection profonde dans les tropiques. Alors que les tendances à long terme des températures observées pendant les événements tropicaux de convection profonde ont été précédemment documentées, les tendances des températures

de surface au moment de la formation des cyclones n'avaient pas été examinées jusqu'à présent. Ces tendances à long terme représentent donc un changement anthropogénique de l'activité cyclonique nouvellement détecté. Le réchauffement observé à la surface des océans au moment de la formation des cyclones est principalement dû au réchauffement des océans avec le temps, ce qui est légèrement contrebalancé par l'effet de la migration des trajectoires des cyclones vers des régions climatologiquement plus froides. Enfin, des simulations de conditions climatiques zonalement asymétriques, avec différentes concentrations en $CO_2$, montrent que la fréquence des cyclones tropicaux est particulièrement sensible au déplacement méridional de la zone de convergence intertropicale et, dans une moindre mesure, aux variations des températures de surface de l'océan. Dans les simulations, la réponse à l'échelle locale des variables environnementales (température et précipitation) et de la fréquence des cyclones tropicaux dans la région froide est plus marquée que la réponse dans la région chaude. Ceci entraîne donc une diminution du nombre global de cyclones tropicaux et d'ouragans, par rapport à des conditions climatiques zonalement symétriques.

TABLE OF CONTENTS

LIST OF TABLES

LIST OF FIGURES

# CHAPTER 1
# Introduction

## 1.1 General overview

### 1.1.1 Tropical cyclones

Tropical cyclones (TC) are ones of the most dangerous natural disasters (*Emanuel*, 2003). They have been detected and observed over the course of the 20th century with improvement from the development of observing technologies, such as satellite remote sensing, which allows more accuracy in their surveillance. In the current climate, about 80 cyclones develop each year in the different ocean basins in the world, mostly in summer or in early autumn. Storms develop over tropical ocean water and move toward higher latitudes until they decay over land or cold water. The maximum wind speed and the central surface pressure of the storm are used as measures of intensity; if the maximum wind speed is higher than 18 m $s^{-1}$, the storm is classified as a tropical cyclone, and if the wind speed reaches 33 m $s^{-1}$, it is classified as a hurricane or a typhoon.

### 1.1.2 Tropical cyclone genesis and environmental conditions

The mechanisms of tropical cyclone genesis are still not clear, however some factors are thought to be favorable to TC genesis. Among them are warm sea surface temperatures (SST), small vertical shear of horizontal wind, and large cyclonic low-level vorticity (*Emanuel*, 2003). Other favorable conditions are high humidity and at least 5° of latitude from the equator, so that the Coriolis effect is strong enough to deflect the winds and create a rotating circulation.

As TC genesis depends on environmental conditions, the cyclonic activity is correlated with climate variations, on seasonal, inter-annual as well as longer time-scales. For instance, El-Niño phenomenon, sub-Saharan rainfall, and North-Atlantic Oscillation modify the vertical wind shear, and thus may alter the frequency of tropical cyclone genesis (*Emanuel*, 2003). Consequently, one can expect that climate change will impact the tropical cyclone activity in the coming century.

### 1.1.3 Global warming

Global warming is an issue of great interest at present. The current state of scientific knowledge regarding climate change is synthesized in the fifth assessment of the Intergovernmental Panel on Climate Change (IPCC) (*Pachauri et al.*, 2014). Some of the working groups assessed the climate change and climate system from a physical point of view and examined the scientific expectations for near-term and long-term climate change (*Kirtman et al.*, 2013; *Collins et al.*, 2013).

The evidence is now clearer that many changes in the climate system since the 1950s have a substantial contribution from anthropogenic forcing. Using the terminology for likelihoods from the IPCC, it is *very likely* that observed increase in upper-ocean heat content and thus in sea surface temperature, is due to anthropogenic forcing (*Stocker*, 2014). In the near-term, the precipitation will *more likely than not* decrease in the subtropics and globally averaged surface and vertically averaged ocean temperatures will *very likely* keep increasing (*Kirtman et al.*, 2013). Over the $21^{st}$ century, if the level of greenhouse gases (GHG) emissions stays unchanged, the global mean temperatures will continue to increase with regionally inhomogeneous changes. Similarly, precipitation will globally increase with some spatial variations, *very likely* resulting in higher contrasts between wet and dry seasons and wet and dry regions. In all scenarios, sea surface temperatures will also increase (*Collins et al.*, 2013). The projections of temperatures and precipitation, in the global mean or averaged over large areas, are of high confidence. However, there are still some uncertainties in projections of near-term climate, on local and global scales, with the high uncertainty in projections of aerosol concentration as an important contributor.

## 1.2 Research objectives

The overall objective of this research is to better understand the effect of environmental conditions, and sea surface temperature in particular, on tropical cyclone genesis. The specific objectives are to:

- Re-examine the concept of a SST threshold for tropical cyclone genesis across ocean basins.

- Evaluate the adequacy of SST and of vertical difference in equivalent potential temperature as TC genesis predictor.
- Assess the trends in SST at TC genesis and compare them to those of the summer environment.
- Examine all tropical deep convective events and the trends in SST at their genesis.
- Evaluate the response of TC frequency to zonally asymmetric environmental conditions.

## 1.3 Organization of thesis and contribution of authors

The following remarks serve as a guide in reading this manuscript-based thesis.

Chapter 1 provides an introduction to this thesis and presents the research objectives and the thesis structure.

Chapter 2 provides a detailed literature review on tropical cyclone genesis, global warming, and the impact of climate change on tropical cyclone activity.

Chapters 3 and 4 are two manuscripts that address the research objectives listed above. The manuscript in Chapter 3 has been submitted to *Geophysical Research Letters* and analyzes the distribution of environmental variables (SST and vertical difference in equivalent potential temperature) at tropical cyclone genesis and during summer, across ocean basins. The manuscript in Chapter 4 will be submitted to *Nature Geoscience* and focuses on trends in SST, at tropical cyclone genesis, during deep convection events, and over the summer season. Both manuscripts are the result of a collaborative work with Prof. Merlis. I, Cécile Defforge, performed all of the statistical analysis and idealized numerical simulations. Prof. Merlis provided the initial scripts for idealized numerical simulations and supervised the research. Both T.M.M. and C.D. contributed to the central ideas presented in the paper and wrote the manuscript describing the results.

Chapter 5 addresses the question of the response of tropical cyclone genesis to zonally asymmetric environmental conditions using high-resolution simulations.

Chapter 6 summarizes the conclusions of the research performed.

# CHAPTER 2
# Literature review

## 2.1 Tropical cyclone genesis and sea surface temperature

Sea surface temperature (SST) is thought to be an important parameter in the development of storms and tropical cyclones. Many studies have analyzed the impact of SST and, more specifically, consider the existence of a SST threshold for cyclogenesis.

### 2.1.1 Convection and upper-tropospheric temperature

Tropical cyclones are one particular form of tropical convection. Consequently in addition to studying cyclogenesis, one can adopt a broader point of view and examine the relationship between SST and tropical convection. The frequency of deep convection can be measured by the probability of low values of outgoing longwave radiation (OLR) or of large fractional coverage of deep convective clouds; the two methods giving similar results (*Zhang*, 1993).

Deep convection is very rare and weak for SSTs less than 26°C, the frequency and intensity of convection increase with SST between 26°C and 30°C such that strong deep convection is highly probable only for SSTs warmer than 28°C. Warm SST is typically a necessary but not sufficient condition for deep convection and the smooth increase of frequency with SST suggests that there is no evidence of a SST threshold necessary for convection (*Zhang*, 1993).

The tight link between convective instability and SST comes from the strong dependence of boundary-layer moist static energy on SST and the weak gradients in upper-tropospheric temperatures (*Johnson and Xie*, 2010; *Sobel*, 2007). The study of a convective threshold, based on the convective available potential energy (CAPE), shows a strong correlation with the mean tropical SST with similar interannual variability and comparable long-term trends of approximately 0.1°C decade$^{-1}$ over the last 30 years (value obtained with the NOAA Extended Reconstruction Sea Surface Temperature data set) (*Johnson and Xie*, 2010). However, the large variability of deep convection at a given

SST suggests that other factors are also important in determining deep convection and casts doubt on the concept of SST "threshold" for deep convection (*Zhang*, 1993).

Another parameter of great importance for convective instability is the upper- tropospheric temperature. It is included in the calculation of potential intensity, which is an upper bound for TC intensity, as measured by maximum surface wind speed (*Emanuel*, 2003). Upper-tropospheric temperatures are one of the major sources of uncertainty in calculations of potential intensity trends (*Emanuel*, 2003; *Vecchi et al.*, 2013). The strong coupling between the mean tropical SST and the SST at location of deep convection, in both observations and models, strengthens the confidence that the warming of the tropical atmosphere is close to a moist-adiabat adjustment(*Sobel et al.*, 2002). Consequently, the SST st location of deep convection gives indications about the trends in upper-tropospheric temperatures under global warming (*Johnson and Xie*, 2010). Another way to estimate the upper-troposphere temperature experienced by TCs is to use tropical cyclones as thermometers. Tropical cyclones trigger strong updrafts nearly reaching the tropopause such that satellite-based remote-sensing temperatures at the top of the clouds can reveal the upper-tropospheric temperatures in the region surrounding the storms, especially in terms of seasonal and interannual variability (*Kossin*, 2015).

### 2.1.2 Global SST threshold for cyclogenesis

Since 1948, it has been commonly accepted that the development of tropical cyclones (TC) requires a minimum threshold SST of 26°C (*Palmen* (1948), *Gray* (1968)). Whereas much research considers multiple environmental factors, recent studies focused only on the SST and re-examined the hypothesis of a SST threshold for tropical cyclogenesis (*Dare and McBride*, 2011; *Tory and Dare*, 2015). They analyzed the distribution of SSTs at the time of TC genesis, i.e., the first time the maximum sustained wind reaches the cyclonic intensity (18 m $s^{-1}$). The recent studies confirmed the value of 25.5°C as an acceptable threshold since 98% of the TCs have developed over warmer SSTs. If one consider the maximum SST encountered by the tropical depression during the 24 hours preceding its genesis, the threshold becomes 26.5°C.

However, there are a substantial number of storms which developed over colder SSTs, especially among the systems undergoing tropical transition from baroclinic precursor disturbances (*McTaggart-Cowan et al.*, 2015). Most of the cold events show a tropopause height lower than usual. A new criterion, called the coupling index, can be defined as a maximum of 22.5°C between the equivalent potential temperatures at the tropopause-level and at 850hPa (*McTaggart-Cowan et al.*, 2015). The coupling index accounts for baroclinically influenced systems so the combination of the usual SST threshold with the coupling index could help improve TC forecasting.

Although previous studies have examined the global distribution of the SST at TC genesis, we performed a regional-scale analysis. The tropical cyclones observed are distributed across the different ocean basins with the five most active ones being West, East, and South Pacific, North Atlantic, and South Indian. The basin-by-basin analysis aims to highlight the differences and similarities that may exist between the basins and examine the robust features of SST at TC genesis.

## 2.2 Impact of climate change on TC activity

The tropical cyclone activity is tightly linked to the environmental conditions and therefore it is expected to change with global warming. Many studies have examined how the TC intensity and frequency have changed and should evolve in warmer climates (*Knutson et al.*, 2010; *Merlis et al.*, 2013; *Zhao et al.*, 2009; *Emanuel*, 2005). The IPCC assesses that there is a degree of consensus about global response of TC activity but the changes in intensity and frequency of TC are of low confidence in near-term basin-scale projections (*Kirtman et al.*, 2013).

### 2.2.1 Effect of global warming on environmental conditions

#### Definition and evolution of the tropical edges

The analysis of tropical cyclone generally requires a definition of the tropical edges in order to exclude non-tropical storms of the study. Some studies used the fixed value of 35° of latitude (*Dare and McBride*, 2011) whereas others defined the tropical boundaries from a dynamical point of view (*Tory and Dare*, 2015; *Davis and Rosenlof*, 2012). In fact the latitudinal extent of the Tropics changes with time on short and longer time scales (*Tory and Dare*, 2015) and several parameters can be used to define the tropical edges.

Different methods use the tropopause height, the tropopause meridional gradient or the mean area-weighted latitude of the tropopause gradient to define the boundaries of the Tropics. Others consider the outgoing longwave radiation (OLR) or the wind jets (*Davis and Rosenlof*, 2012). The tropical edges also correspond to the Hadley cell edges which can be diagnosed examining the mean-meridional streamfunction in the upper troposphere or the difference of precipitation minus evaporation. Both quantities equal zero at the poleward edge of the Tropics.

To avoid biases induced by globally uniform trends or noise, metrics based on the identification of the mean values or zero-crossing thresholds are recommended (*Davis and Rosenlof*, 2012). The tropical widths show increasing trends, at a rate somewhat smaller than 1° latitude per decade, but these trends depend on the reanalysis product, the hemisphere, the method, and the time period considered (*Johanson and Fu*, 2009; *Archer and Caldeira*, 2008; *Davis and Rosenlof*, 2012).

The results presented in Chapter 3 do not change if these objective methods are used.

**Changes in the hydrological cycle**

In addition to changes in SST and precipitation intensity and pattern discussed in 1.1.3, the hydrological cycle may also be affected by global warming. Based on the Clausius-Clapeyron (CC) formula, the saturation vapor pressure increases with a rate of approximately 7 % per Kelvin of warming. The lower-tropospheric water vapor also increases substantially with warming, obeying CC scaling (*Held and Soden*, 2006). As the radiative fluxes have a weaker temperature dependence, the global-mean precipitation increases less than that implied by CC scaling, suggesting that the mass exchange between the boundary layer and the free troposphere decreases rapidly with warming, as well as the convective mass flux. The response of precipitation minus evaporation (P-E) to warmer climate simulated by the models is in good agreement with the thermodynamic component predicted by CC, especially the fact that dry (wet) regions will become even drier (wetter) (*Held and Soden*, 2006).

Climate change also affects the Walker circulation and zonal surface temperature gradients, that can be simulated by an idealized general circulation model (GCM) with an imposed asymmetric ocean energy flux and different values of the optical thickness of an idealized longwave absorber. The idealized simulations show that the zonal surface temperature gradient in the Tropics generally decreases and the Walker circulation weakens with warming (*Merlis and Schneider*, 2011). The changes in the Walker circulation can be accounted for using locally evaluated hydrological cycle scaling estimates. They can be decomposed into equatorial precipitation increases, that are approximately zonally uniform, and rapid increases of saturation specific humidity with warming (*Merlis and Schneider*, 2011).

In Chapter 5 we used a similar experimental design but with a GCM that simulates tropical cyclones, thanks to a finer resolution and a different physical parameterisation.

### 2.2.2 Effect of global warming on TC track

The latitude where tropical cyclones reach their lifetime maximum intensity (LMI) has moved poleward with a global trend of approximately 1° per decade over the last 30 years *Kossin et al.* (2014). This rate of migration is comparable to the one observed for the tropical expansion (2.2.1), which may cause changes in the mean meridional structure of the environmental vertical wind shear and potential intensity. The shift of tropical cyclone activity away from the equator is apparently linked to these changes and appears to have anthropogenic causes (*Kossin et al.*, 2014).

The poleward migration of tropical cyclones may affect the storm-local environmental conditions. In this study we will examine whether the poleward trend is also observed for the latitude of tropical cyclone genesis and how it affects the mean SST at genesis (Chap. 4).

### 2.2.3 Effect of global warming on TC frequency

Observed tropical cyclones during the past decades showed large amplitude fluctuations in their frequency and intensity without significant trends but the projections of future TC activity show some changes that are robust among the different models (*Emanuel*, 2003; *Bengtsson et al.*, 2007; *Emanuel et al.*, 2008; *Sugi et al.*, 2009; *Zhao et al.*, 2009; *Knutson et al.*, 2010; *Held and Zhao*, 2011; *Emanuel*, 2013; *Merlis et al.*, 2013; *Zhao and Others*, 2013; *Merlis et al.*, 2016).

There is a degree of consensus about the trend in globally-averaged TC frequency that is decreasing or neutral, except for the strongest TCs that are more frequent with greenhouse warming (*Knutson et al.*, 2010; *Bengtsson et al.*, 2007; *Emanuel et al.*, 2008; *Merlis et al.*, 2016).

The reduction in the global number of TCs in future climate simulations is due to both the increase in $CO_2$ concentration and the warming of SSTs (*Held and Zhao*, 2011; *Zhao and Others*, 2013). The response to the doubling of $CO_2$ is more robust among models than the response to the increase in SST (*Zhao and Others*, 2013) and the relative importance of the contribution of $CO_2$ is larger in the Northern Hemisphere than in the Southern Hemisphere (*Held and Zhao*, 2011). In these simulations the changes in TC genesis frequency seem to be due to changes in the convective mass fluxes (*Held and Zhao*, 2011; *Zhao and Others*, 2013).

Furthermore, the increase of greenhouse gases concentration triggers a poleward shift of the ITCZ and modifies the TC frequency (*Merlis et al.*, 2013). The TC frequency decreases due to warming, with fixed ITCZ latitude, and increases due to the poleward shift of the ITCZ, with unchanged tropical-mean SST. The relative importance of each phenomenon impacts the sign of the change in TC frequency and can lead to increasing trend (*Merlis et al.*, 2013).

While most of the future climate change scenarios show a reduced global number of TCs, some simulations give positive trends (*Merlis et al.*, 2013; *Emanuel*, 2013), that is consistent with the increase of the genesis potential index forecasted based on monthly-mean global model output (*Emanuel*, 2013). Moreover, the accuracy in the prediction of tropical cyclone activity increases globally, but the projections for individual basins show large discrepancies between different modeling studies (*Sugi et al.*, 2009; *Knutson et al.*, 2010). For example, the comparison of observed counts of hurricanes and simulated annual frequency by a GCM with prescribed SSTs shows a strong correlation for the Atlantic basin. This indicates that Atlantic hurricane inter-annual variability is explained quasi-exclusively by variations in SST whereas the correlations are lower to insignificant in the other basins (*Zhao et al.*, 2009). It is in this context that we examine the distribution and long-term trends of SST at TC genesis across ocean basins, in order to study which results are robust among the basins.

In the last part of our study, we will simulate the response in TC frequency to asymmetric environmental conditions. Global circulation model (GCM) with prescribed SSTs give good results in simulating climatology and interannual variability of tropical storm frequency, even if the distribution of intensities is not necessarily realistic (*Zhao et al.*, 2009). Consequently we will use a GCM in our study and prescribe energy fluxes at the boundary between ocean and atmosphere, that is directly linked to SST.

### 2.2.4 Effect of global warming on TC intensity

The effect of global warming on TC intensity is still poorly understood but most of the studies agree on a increasing trend in future climate projections (*Emanuel*, 2003; *Held and Zhao*, 2011; *Merlis et al.*, 2016; *Emanuel*, 2005).

Over the past 30 years, there has been a lack of trend in storm-local environment conditions, especially regarding outflow temperatures (*Kossin*, 2015). Based on the potential intensity theory (*Emanuel*, 2003), the lack of trend in potential intensity implies that mean tropical cyclone intensity should not have increased over the past 30 years, consistently with observed global intensity trends. The nearly stable trend in potential intensity is explained by the fact that the potential intensity mean state increases with time in the regions where storms develop, which is compensated by the decrease due to poleward migration of storm tracks (*Kossin*, 2015).

In projections of future climate, the globally averaged intensity of tropical cyclones increases with greenhouse warming, shifting towards stronger storms (*Held and Zhao*, 2011; *Bengtsson et al.*, 2007). In fact, the increase in TC intensity is mainly due to the warming of SSTs and the increase in surface specific humidity whereas the doubling of $CO_2$ concentration does not seem to play an important role (*Held and Zhao*, 2011;

*Bengtsson et al.*, 2007). This increase is enhanced by the projected increase in storm lifetime with warming (*Emanuel*, 2005).

### 2.2.5 Effect of SST pattern and relative warming

The global and regional TC frequencies are sensitive to regional SST changes pattern (*Zhao et al.*, 2009; *Sugi et al.*, 2009). In particular, there is a strong correlation between the Atlantic hurricane frequency and the differential warming of SSTs in the Atlantic main development region with respect to the SST averaged over the entire tropical ocean (*Zhao et al.*, 2009; *Swanson*, 2008). Consequently, the Atlantic intensity fluctuations and TC frequency depend on both the local SST anomalies and the tropical mean SSTs (*Swanson*, 2008). In fact, the differential warming affects the static stability over the Atlantic as well as the vertical shear making the environment more favorable to TC development and intensification (*Zhao et al.*, 2009). Using averaging times longer than a year, the correlation between Atlantic hurricane frequency and SST is better if one considers relative SSTs rather than absolute SST values (*Vecchi et al.*, 2008), where relative SST is defined as the departure from the tropical mean SST. The increase in relative SST in the Atlantic over the last decades could be only due to internal climate variability and should not continue increasing in the future. In this case, the future of TC genesis would be comparable to that observed in the late decades (*Vecchi et al.*, 2008).

Geographical contrasts in warming may come from changes in the seasonal cycle. The surface wind speeds decrease in the summer hemisphere, leading to a warming with respect to the global mean (*Sobel and Camargo*, 2011). The increase in the seasonal SST contrasts is associated with substantial increase in precipitation and in convective available potential energy (CAPE) in summer hemisphere. The changes in SST, precipitation, CAPE, and TC potential intensity (PI) are due to both the annual mean changes and the seasonal changes, in comparable fractions (*Sobel and Camargo*, 2011). Furthermore the net changes between the 20th and 21st centuries are greater in July-August-September, when the seasonal changes enhance the annual-mean changes, than in January-February-March (*Sobel and Camargo*, 2011). The seasonally varying changes potentially affect the

TC activity differently in Northern Hemisphere (NH) basins than in Southern Hemisphere (SH) ones.

However, the SST or relative SST is not in and of itself a good environmental predictor for TC genesis as surface wind speeds and surface energy fluxes play an important role in determining environmental factors such as potential intensity (PI) (*Emanuel and Sobel*, 2013).

The effect of global warming on TC activity is a very broad topic with many uncertainties due to the unclear mechanisms involved in tropical cyclone genesis. Here we focus only on the frequency of tropical cyclones and its sensitivity to environmental parameters. First, we examine the trends in the observed TC genesis events over the past 30 years, performing a basin-by-basin analysis (Chapters 3 and 4). Furthermore, we simulate a zonally asymmetric climate to examine how the tropical cyclone frequency responds to such environmental conditions (Chapter 5).

CHAPTER 3

# Distribution of sea surface temperature at tropical cyclone genesis across ocean basins

**C. Defforge[1] and T. M. Merlis[1]**

[1]*Department of Atmospheric and Oceanic Sciences, University of McGill, Montreal, Quebec, Canada.*

Submitted to *Geophysical Research Letters*

### 3.1 Introduction

After World War II, scientists proposed a sea surface temperature (SST) threshold of 26$^o$C as a necessary condition for tropical cyclone (TC) genesis (*Palmen*, 1948; *Gray*, 1968). Subsequent research has revealed that other thermodynamic variables are more directly associated with TC intensity (*Emanuel*, 1995, 2003; *Emanuel and Nolan*, 2004), such as potential intensity (PI) and surface enthalpy flux, and these have subsequently been used predictor variables in multi-variate "genesis potential indices" (*Camargo et al.*, 2007a,b; *Tippett et al.*, 2011). Furthermore, a threshold SST in the current climate is not likely to be relevant in a perturbed climate (as is understood for the case of moist convection in the tropics (*Graham and Barnett*, 1987; *Zhang*, 1993; *Johnson and Xie*, 2010)), so the utility of such a threshold in the out-of-sample case of interest—climate change—is suspect. Indeed, simulations of TCs in perturbed climate states do not show geographic or frequency changes that would be expected from a fixed SST threshold for genesis (*Bengtsson et al.*, 2007; *Emanuel et al.*, 2008; *Sugi et al.*, 2009; *Zhao et al.*, 2009; *Knutson et al.*, 2010; *Merlis et al.*, 2013; *Zhao and Others*, 2013; *Merlis et al.*, 2016).

In spite of the wealth of physical reasoning and numerical simulations that argue against the relevance of a SST threshold for TC genesis, recent works have revisited the existence of a TC genesis SST threshold with contemporary data sets for the era of satellite observations (*Dare and McBride*, 2011; *Tory and Dare*, 2015). These studies have confirmed the existence and value of SST threshold of 26$^o$C that had been suggested decades earlier. In light of this apparent disconnect between these observational studies, and physical reasoning and numerical simulations, we re-examine observations of SST at time of TC genesis (hereafter referred as SST$_G$) to assess the observational support for a global SST threshold.

We examine three dimensions of this question. First, to what extent does a 'global' threshold arise from regional variations? *McTaggart-Cowan et al.* (2015) recently examined the different TC development pathways that commonly occur at cold SSTs (<26.5$^o$C). The cold events analyzed in their study happened either in the North Atlantic basin or at the poleward edge of other basins and almost never occur in the West

Pacific basin. In the present study, we examine if the location of these cold events can be explained by climatological differences between the basins, rather than closely analyzing differences in meteorological features. Second, to what extent is the probability density function (PDF) of $SST_G$ have a sharp increase with SST as the word “threshold” might indicate? Third, to what extent is the PDF of $SST_G$ shaped by the environmental conditions of the main development region (MDR)? For example, TC genesis is not observed at SSTs greater than $32^o$C simply because SSTs are never this warm, providing an environmental upper bound on $SST_G$. Therefore, we compare the environment's SST distribution during the whole TC season (hereafter referred as $SST_S$) to that observed during genesis.

### 3.2 Data

We use the tropical cyclone track information from release v03r08 of the International Best Track Archive for Climate Stewardship (IBTrACS) database (*Knapp et al.*, 2010) which is composed of data from 11 tropical cyclone observation centers since 1842, including the position and a near-surface wind speed estimate every 6 hours of the storm track. The IBTrACS database also indicates the nature of the storm (for example, “tropical”, “subtropical”, “extratropical”, etc.), as determined by the individual regional specialized meteorological centers (RSMC), when available.

The storm tracks are combined with the $1/4^o$ daily Optimum Interpolation Sea Surface Temperature (OISST) data set (*Reynolds et al.*, 2007) from the National Oceanic and Atmospheric Administration (NOAA) to determine the genesis SST. This data set provides daily mean values of SST with a horizontal resolution of $0.25^o$ from 1982 to the present.

We also use data from the Modern-Era Retrospective analysis for Research and Applications (MERRA) (*Rienecker et al.*, 2011) to assess the atmosphere's vertical stability. MERRA is a NASA atmospheric reanalysis for the satellite era that derives the sea surface boundary condition from the $1^o$ resolution NOAA/OISST product and has a horizontal resolution of $2/3^o$ longitude by $0.5^o$ latitude and 2 hour temporal resolution.

### 3.3 Methodology

The present study is performed over the 33-year period from 1982 to 2014 (the period covered by both the OISST and IBTrACS data sets). All the storms which developed during this period are filtered in order to study only those which reach tropical cyclone intensity within the Tropics. The *genesis* of the tropical cyclone is defined as the moment when the estimated winds of the storm exceed 18 m $s^{-1}$ (35 knots). The filtering of tropical storms according to the morphology involves the storm's nature, assigned by the RSMC that recorded it (*Dare and McBride*, 2011). Consistent with previous studies, we excluded the storms that are not labeled as "tropical" in the IBTrACS database and those that developed at latitudes poleward than $35^o$ (*Dare and McBride*, 2011; *Tory and Dare*, 2015). Some other methods based on dynamical criteria, such as the subtropical jet position, may be used to distinguish tropical from non-tropical storms (*Tory and Dare*, 2015). We investigated alternative methods that only consider the latitude at the time of TC genesis and that define the boundaries of the Tropics accordingly to dynamical criteria. However, the $SST_G$ distributions are not sensitive to the method used to exclude non-tropical storms, so only the one using IBTrACS labels is presented here, following *Dare and McBride* (2011).

For the selected tropical cyclones, we linearly interpolate the SST between daily means to the time of genesis and average meridionally the SST over a $1.5^o$ latitude radius, following *McTaggart-Cowan et al.* (2015). The storms are sorted according to the basin in which they developed and the five most active basins are examined here: West Pacific (WP, 1072 TCs examined), East Pacific (EP, 668 TCs), South Indian (SI, 504 TCs), North Atlantic (NA, 495 TCs), and South Pacific (SP, 390 TCs). The other basins are excluded from the analysis because of the small number of TCs and, in the North Indian ocean basin, the TC nature is frequently not reported in IBTrACS. The probability distributions are obtained using averaged shifted histograms with bins of $0.5^o$C width, shifted by $0.49^o$C (*Scott*, 2010). On the plots, the x-value corresponds to the center of the bin and the y-value is the percentage occurrence of the SSTs contained in the bin.

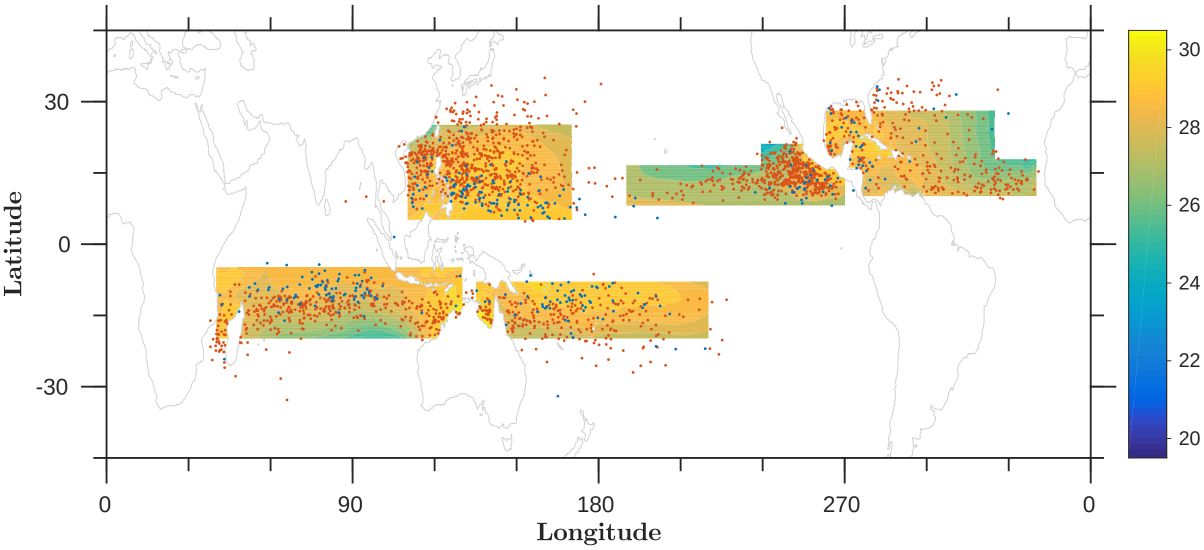


Figure 3–1: Spatial extent and seasonal-mean SST contours for each basin, and location of the cyclogenesis events. For each basin, SSTs are averaged over the tropical cyclone seasons between 1982 and 2014: WP (Jun-Nov), EP (Jun-Oct), NA (Jul-Oct), SI (Dec-Apr), SP (Jan-Apr). The cyclogenesis events that occurred during the TC season are shown in red and others are shown in blue.

For each basin, the sea surface temperatures throughout its 33 tropical cyclone seasons are also examined, hereafter referred as $SST_S$. Figure 3–1 shows the spatial extent of each basin and the months that define the TC season. They correspond to the main development period and region, and are similar to those used by *Wing et al.* (2015). As in our analysis of $SST_G$, the values of $SST_S$ are sorted in bins of 0.5$^o$C using averaged shifted histograms.

In addition to the local sea surface temperature, the relative SST (RSST) and a vertical difference in equivalent potential temperature are also examined as the former is often used in the construction of genesis potential indices (*Tippett et al.*, 2011) and the latter is a measure of atmospheric convective instability. The relative SST is defined as the departure from the tropical mean SST, calculated with monthly-mean values between 20$^o$S and 20$^o$N, following *Tippett et al.* (2011). The equivalent potential temperature ($\theta_e$) is computed from MERRA reanalysis using Bolton's formula (*Bolton*, 1980). We calculated the equivalent potential temperature at TC genesis and for the basin TC seasons at 10 m above the sea surface level and at 500 hPa (see Appendix A for more information). We also computed the difference between the upper- and lower-level equivalent potential temperature for both TC genesis and TC season environment (respectively referred as $\delta\theta_{e,G}$ and $\delta\theta_{e,S}$). The occurrence distributions are obtained following the same method as used for $\mathrm{SST}_G$ and $\mathrm{SST}_S$.

The statistical distance between probability distributions of $\mathrm{SST}_S$ and $\mathrm{SST}_G$ or between distributions of $\mathrm{RSST}_S$ and $\mathrm{RSST}_G$, or between $\delta\theta_{e,G}$ and $\delta\theta_{e,S}$, is measured here by the Bhattacharyya distance (*Bhattacharyya*, 1943). This distance is related to the Bhattacharyya coefficient, that measures the amount of overlap between two statistical distributions. As an example, a distance of zero indicates identical distributions and two normal distributions with the same standard deviation of $1^o$C (a typical value of standard deviation for $\mathrm{SST}_G$ distributions), and means that differ by $1^o$C have a distance of 0.125.

## 3.4 Results

### 3.4.1 Analysis of SST at TC genesis

Figure 3–2 shows the cumulative distributions of the sea surface temperature at tropical cyclone genesis, $\mathrm{SST}_G$, for each ocean basin separately. It also shows the global distribution of $\mathrm{SST}_G$ (thick black line), reproducing the results of *Dare and McBride* (2011) and *Tory and Dare* (2015). The basins show different characteristics regarding $\mathrm{SST}_G$, with North Atlantic being the coldest basin and West Pacific the warmest one. The values for the $5^{th}$ percentile correspond to the SST such that 95% of the tropical cyclones observed between 1982 and 2014 developed over warmer SSTs (Fig. 3–2b). These values range between 25.7$^o$C for the North Atlantic, 26.4$^o$C for the global distribution, and 27.0$^o$C for the West Pacific. The substantial variability between the basins — more than $1^o$C — indicates that the SST "threshold" necessary for TC genesis is basin dependent. For percentiles smaller than 10%, all the basins, except the North Atlantic, are either similar to, or warmer than, the global $\mathrm{SST}_G$ values. Consequently, the North Atlantic basin shifts the low percentiles of the global SST distribution at TC genesis toward colder temperatures.

The impact of using a globally defined SST threshold therefore varies by basin. In the North Atlantic, a 26$^o$C "threshold" is too restrictive leading to an increased number of missed development events. Conversely, a 26$^o$C "threshold" is not sufficiently stringent

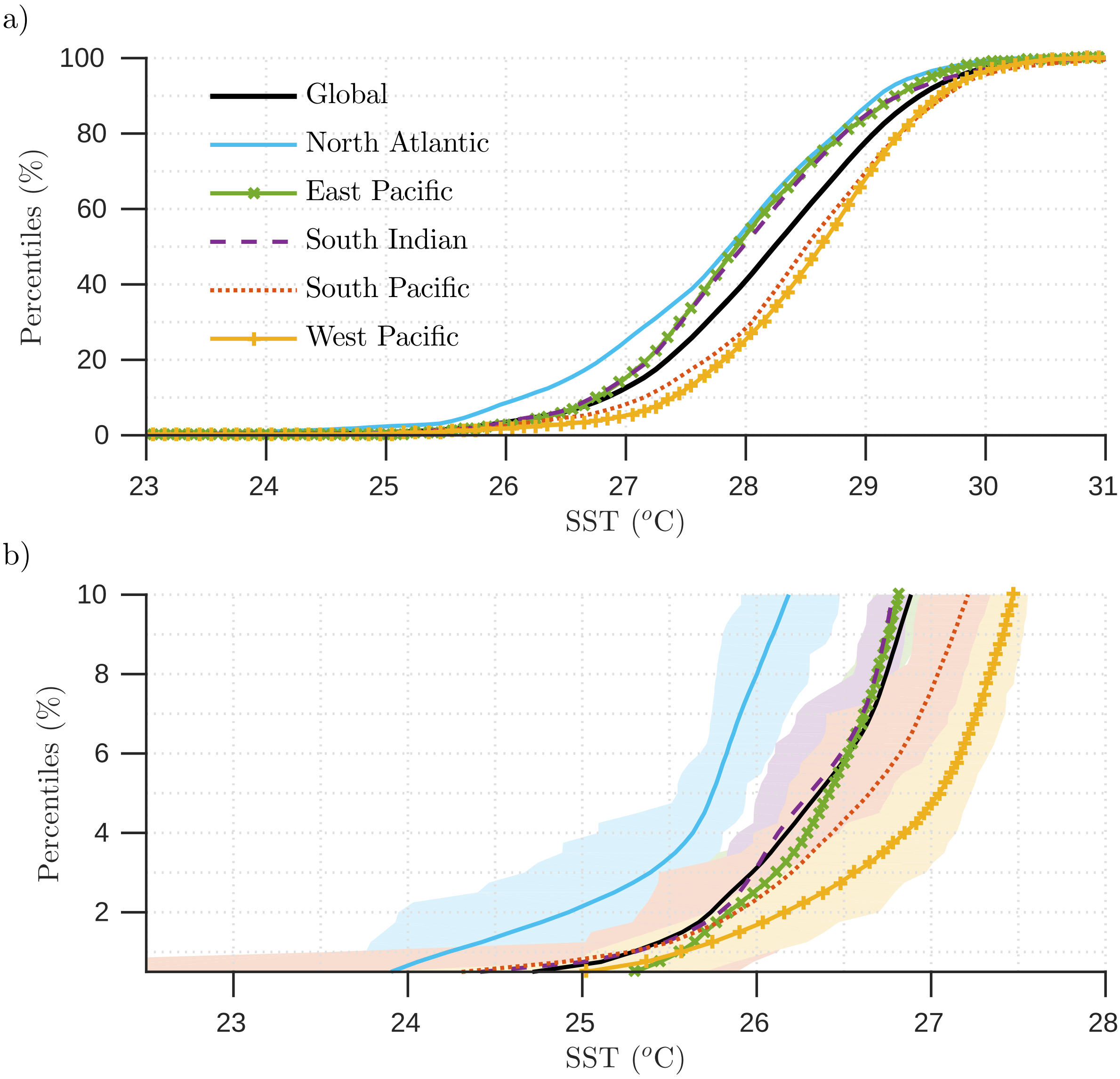


Figure 3–2: Cumulative distribution of the SST at the time of TC genesis ($SST_G$), for each ocean basin separately (colored lines indicated in the legend) and for the globe (thick black line) for (a) the full distribution and for (b) the lowest percentiles with 95% confidence interval (shaded). The bootstrapping method used to obtain the SST values for the percentiles and the corresponding confidence interval is described in the Appendix A (A1).

Table 3–1: Values of the skewness of the distributions of SST at TC genesis ($SST_G$). Negative values indicate that the tail on the left side is fatter than the right side.

| **Basin** | **Skewness** |
|---|---|
| NA | -0.72 |
| WP | -0.75 |
| EP | -0.17 |
| SP | -0.6 |
| SI | -0.38 |
| Global | -0.59 |

in the West Pacific basin leading to an increased number of false alarms. Thus basin-specific analysis is clearly required to maximize the utility of SST as a criterion for TC developments.

The shape of the cumulative distributions of $SST_G$ across the ocean basins (Fig. 3–2) suggests that the probability distribution functions of $SST_G$ are nearly symmetrical. Table 3–1 gives the skewness of the $SST_G$ distribution for each basin (solid line), which is a measure of the asymmetry of the probability distributions. For all the basins, the values of skewness are negative, indicating that their left tails are longer than the right ones. This stands in contrast to the concept of a threshold that would expect an abrupt increase in cumulative occurrences at a certain value of SST. Even from a basin-specific perspective, the occurrences of $SST_G$ increase smoothly with SST in the cold tail of the distribution and decrease smoothly in the warm tail. Taken together, the results cast doubt on the concept of a global SST threshold necessary for TC genesis.

### 3.4.2 Comparison with SST over the tropical cyclone season

In order to compare the SST at TC genesis with the climatological environmental conditions observed at ocean's surface, we computed the distribution of the SST over the tropical cyclone season of each basin, referred as $SST_S$. The months corresponding to the tropical cyclone season in each basin are considered, because the other environmental parameters influencing TC genesis, such as the vertical wind shear or free-tropospheric humidity (*Gray*, 1968; *Nolan and McGauley*, 2012; *Emanuel*, 2003; *Tippett et al.*, 2011), are generally more favorable during the TC season. The TC genesis events considered in this section and the next one are limited to those that occur within the geographic extent

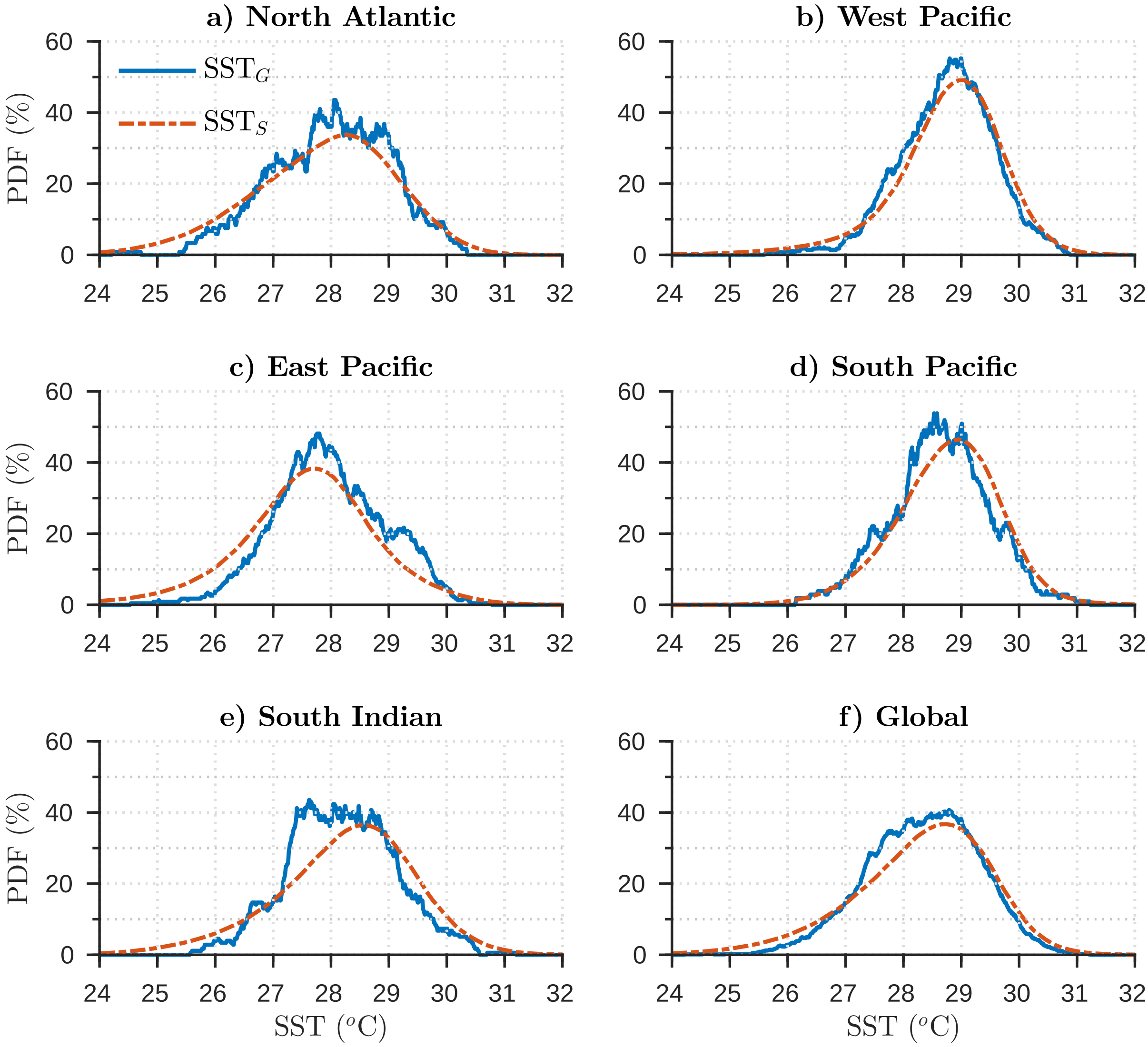


Figure 3–3: Probability distribution function of the SST at TC genesis (SST$_G$) (thick blue line) and of the SST observed during the TC season (SST$_S$) for each basin (dash-dotted orange line): a) North Atlantic basin, b) West Pacific basin, c) East Pacific basin, d) South Pacific basin, e) South Indian basin, f) Global.

and TC season of the basin as shown in Figure 3–1. These temporal and geographic criteria are satisfied for more than 65% of genesis events for all the basins and allow a fair comparison of the environmental climatology and the corresponding genesis events.

Figure 3–3 shows the PDF of $\mathrm{SST}_G$ and $\mathrm{SST}_S$ for each basin. The PDF of $\mathrm{SST}_S$ contains $10^6$ more samples than $\mathrm{SST}_G$: TC genesis is, of course, a rare event. Within each basin, $\mathrm{SST}_G$ and $\mathrm{SST}_S$ span the same range of values, suggesting that the warm and cold bounds of the $\mathrm{SST}_G$ distribution are largely determined by the climatological bounds of the basin's SST. It can be seen that the most frequent $\mathrm{SST}_G$ is equal or colder than the peak of $\mathrm{SST}_S$ occurrence. This indicates that the SST at which TC genesis is the most likely is within the cold-half of the range of SST encountered during the TC season. This is not the case in the East Pacific basin where the $\mathrm{SST}_S$ distribution is slightly shifted to warmer values. Figure 3–3 also shows that the standard deviation is generally slightly smaller for $\mathrm{SST}_G$ than for $\mathrm{SST}_S$. It indicates that during TC season, when the other parameters influencing TC genesis are favorable, increasing the SST from cold values is favorable for TC genesis,as expected. The increase of TC genesis probability with SST seems to saturate at a certain basin-dependent temperature, that is generally colder than the TC season basin mean. For warmer temperatures the likelihood of genesis is nearly insensitive to SST, except for the East Pacific basin where genesis likelihood keeps increasing at warm SSTs. A physical explanation for this saturation in probability at high SSTs could come from the anti-correlation between SST and the Coriolis parameter at low latitudes. Moreover, at high SSTs the middle troposphere also warms such that the atmospheric instability is reduced and genesis is less likely (*Holland*, 1997).

### 3.4.3 Analysis of other environmental parameters: relative SST and vertical gradient in equivalent potential temperature

As the distribution of absolute $\mathrm{SST}_G$ generally resembles the TC season environment, we analyze other environmental parameters that are related to tropical cyclogenesis to see if there distributions at TC genesis are more distinct from climatological environmental conditions and would thus serve as a more sensitive criteria for TC genesis prediction. We thus examined the relative SST (RSST) and the vertical difference in equivalent potential temperature ($\delta\theta_e$).

Table 3–2: Values of the Bhattacharyya distance between the distributions during TC season and at TC genesis for local sea surface temperature (SST), for SST relative to the monthly, tropical mean (RSST), and for difference between upper- and lower-equivalent potential temperature ($\delta\theta_e$). $\Delta$ is the ratio of the distance for RSST or $\delta\theta_e$ distributions to the distance for local SST.

| **Basin** | **SST** | **RSST** | $\delta\theta_e$ | $\Delta_{RSST}$ | $\Delta_\theta$ |
|---|---|---|---|---|---|
| NA | 0.026 | 0.061 | 0.032 | 2.36 | 1.23 |
| WP | 0.013 | 0.036 | 0.022 | 2.82 | 1.77 |
| EP | 0.032 | 0.055 | 0.042 | 1.7 | 1.31 |
| SP | 0.01 | 0.048 | 0.077 | 4.67 | 7.5 |
| SI | 0.032 | 0.059 | 0.081 | 1.84 | 2.55 |
| Global | 0.014 | 0.023 | 0.019 | 1.71 | 1.43 |

Table 3–2 shows the values of the Bhattacharyya distance between the probability distributions at TC genesis and over the main development regions (MDR), for local SST, relative SST (RSST), and the vertical difference in equivalent potential temperature ($\delta\theta_e$). The table also includes the ratio of the distances for RSST and $\delta\theta_e$, compared to the distance for local SST. It can be seen that for all the basins, the distance for RSST is more than 1.5 times larger than for local SST and it is often more than twice as large. The distances for $\delta\theta_e$ are generally somewhat smaller than those obtained with RSST and particularly high for the South Pacific basin. Higher distances between $\text{RSST}_G$ and $\text{RSST}_S$ distributions correspond to less amount of overlapping, suggesting that $\text{RSST}_G$ distribution is more distinct from $\text{RSST}_S$ distribution than $\text{SST}_G$ from $\text{SST}_S$ distributions.

However, these distances are small and the relative SST or the difference in equivalent potential temperature cannot be used in isolation to predict TC genesis but have to be combined with other environmental variables (*Tippett et al.*, 2011).

### 3.5 Conclusions

This examination of the distribution of SST at TC genesis shows that all the ocean basins have their own characteristics. The range of observed SSTs at TC genesis, the mean SST value, and the coldest SST for which TC genesis occurs differ from one basin to another. The differences between the basins suggest that an apparent global threshold SST for TC genesis arises from averaging over the climatologically coldest basins, with the North Atlantic basin accounting for the coldest genesis events. The fact that TC genesis occurs over different ranges of SSTs, according to the basin considered, also indicates that the co-variance of SST with other environmental parameters that are important for TC formation (e.g., vertical shear and humidity) differs between the basins.

The comparison of the occurrences of the SST at the time of TC genesis and the occurrences of SST observed during the entire TC season shows that increasing SST favors TC genesis only for the coldest of the environmental SSTs. Within each basin all the SSTs warmer than the TC season mean have similar probabilities of TC genesis, except for the East Pacific basin where genesis is more likely at warmer temperatures. This comparison also suggests that cold and warm bounds of the SST distribution at TC genesis are largely determined by the climatological SST extrema encountered by the basin during its TC season. A straightforward explanation for the differences between SST at tropical cyclogenesis between ocean basins is that they reflect differences in the TC season environment. This environmental explanation is complementary to the body of literature examining differences in genesis pathways. The extent to which TCs develop from baroclinic precursors, tropical depressions, or convectively coupled waves also have documented geographic variations (*Schreck et al.*, 2011; *Payne and Methven*, 2012; *McTaggart-Cowan et al.*, 2008, 2015).

The analysis of the distributions of relative SST and of the vertical difference in equivalent potential temperature show greater differences between genesis events and the seasonal environment. This confirms that relative SST and difference in equivalent potential temperature are better variables to be used in the construction of genesis potential indices than local SST.

### 3.6 Acknowledgments

The Sea Surface Temperature data used in this study was acquired from NOAA's daily Optimum Interpolation Sea Surface Temperature (https://www.ncdc.noaa.gov/oisst). We acknowledge NOAA for providing the OISST data set and the IBTrACS database (http://www.ncdc.noaa.gov/ibtracs). We also thank the Global Modeling and Assimilation Office (GMAO) and the GES DISC for the dissemination of MERRA (http://disc.sci.gsfc.nasa.gov/daac-bin/DataHoldings.pl). We are grateful for the support of Stephen and Anastasia Mysak Graduate Fellowship (C.D.) and the support of

NSERC Discovery Grant (T.M.). We would like to thank an anonymous reviewer and Dr. McTaggart-Cowan for their constructive comments.

## Connecting text: Chapter 3 and Chapter 4

In Chapter 3, the analysis of the SST distribution at tropical cyclone genesis shows that there is no substantial difference with respect to SST distribution observed in summer environment. The mean SST at TC genesis is therefore close to the mean summer-season SST. In the context of climate change, it is of interest to examine if there are also similarities in the long-term trends of SST at TC genesis and in summer environment. These SST trends are also compared to those observed for all tropical deep convection events to assess whether TC genesis events have distinct environmental trends relative to less extreme, more frequent convection events. These trend analyses and comparison are presented in Chapter 4, using similar analysis techniques and data sets as in Chapter 3.

CHAPTER 4

# Long-term trends in sea surface temperature at TC genesis and for all tropical deep convection events

**C. Defforge**[1] **and T. M. Merlis**[1]

[1]*Department of Atmospheric and Oceanic Sciences, University of McGill, Montreal, Quebec, Canada.*

To be submitted to *Nature Geoscience*

**Tropical cyclone (TC) activity is influenced by several environmental parameters (*Emanuel*, 2003) and it is therefore expected to respond to anthropogenic climate change (*Knutson et al.*, 2010; *Zhao et al.*, 2009; *Merlis et al.*, 2013; *Emanuel and Sobel*, 2013). However, there is observational uncertainty in historical changes in TC activity and attributing observed TC changes to anthropogenic forcing is difficult in the presence of internal climate variability (*Knutson et al.*, 2010). A well-observed environmental factor that affects TC intensity and rainfall is the tropical sea surface temperature (SST), which has a warming trend attributable to anthropogenic activity (*Knutson et al.*, 2013; *Santer et al.*, 2006). Here we show that the sea surface temperature at the time of TC genesis has a significant warming trend over the three decades of the satellite-era when both TCs and SST are well observed throughout tropics. The trend in SST at TC genesis is comparable to the trend in SST during other tropical deep convection events and the trend in SST in the TC main development regions throughout the TC season. This newly documented, observed signature of climate change on TC activity is also present in high-resolution global atmospheric model simulations that explicitly simulate TCs.**

Environmental conditions affect various aspects of the tropical cyclone (TC) activity, such as TC frequency, intensity, and precipitation. Physical reasoning and numerical simulations lead to expectation of changes in tropical cyclone activity under climate change (*Knutson et al.*, 2010; *Merlis et al.*, 2013; *Zhao et al.*, 2009; *Emanuel*, 2005). However, there are difficulties validating the expected response of tropical cyclone in observations. TCs are rare events (about 80 per year globally) with substantial year-to-year variation in their statistics. It is, therefore, difficult to separate internal variability from forced TC changes. Moreover, the global TC distribution has only been well documented since 1979 because the pre-satellite observing network did not have complete spatial coverage.

One of the environmental parameters that influences tropical cyclone activity is sea surface temperature (SST). SST is well observed, though there are some discrepancies between the long- term trends in different datasets (*Flannaghan et al.*, 2014). In the tropics, SST has significantly warmed over the 20$^{th}$ century, and this warming has been attributed to anthropogenic climate change (*Knutson et al.*, 2013; *Santer et al.*, 2006). It has been established that there is a warming trend in the SST during deep convection events (hereafter referred as $SST_{conv}$) that is comparable to the rate of tropical-mean SST warming (*Johnson and Xie*, 2010), and *Dare and McBride* (2011) noted that the SST during TC genesis events was warmer after 1995 than it was before 1995, though they did not quantify the significance of the observed change. Here we perform an examination of the trends in SST at TC genesis and for TC season environment over the five basins with the most TC activity (North Atlantic (NA), East Pacific (EP), West Pacific (WP), South Pacific (SP), and South Indian (SI)) from 1982 to 2014 using the datasets described in the Methods section. We show that the trends in the SST at the time of tropical cyclone genesis (referred to as $SST_G$ in what follows) are significant in the tropical mean and in many individual ocean basins over the satellite era.

Figure 4–1 shows the time series of annual values of the SST at tropical cyclone genesis ($SST_G$) and SST observed during TC season over the main development regions ($SST_S$), averaged over these five basins. Both $SST_G$ and $SST_S$ have warming trends that are statistically significant at the 5% level with a similar rate of about 0.2 $^o$C decade$^{-1}$ in the NOAA OISST dataset. The trend in $SST_G$ is similar if the monthly mean SST is used rather than the daily values (Fig. B–1). The magnitude of the trends is somewhat smaller in NOAA's lower resolution OISST dataset and about half as large in the HadISST dataset (*Rayner et al.*, 2003) (Fig. B–1 & B–2). This dataset dependence of the trends is consistent with model-based analysis of the difference in these two datasets' SST trends in tropical regions with substantial precipitation (*Flannaghan et al.*, 2014). While there is a dataset dependence in the magnitude of the trends, the trends are significantly different from zero in all datasets: the SST at the time of TC genesis has warmed over the last 30 years at a rate comparable to that of the main development regions (MDR) during the TC season.

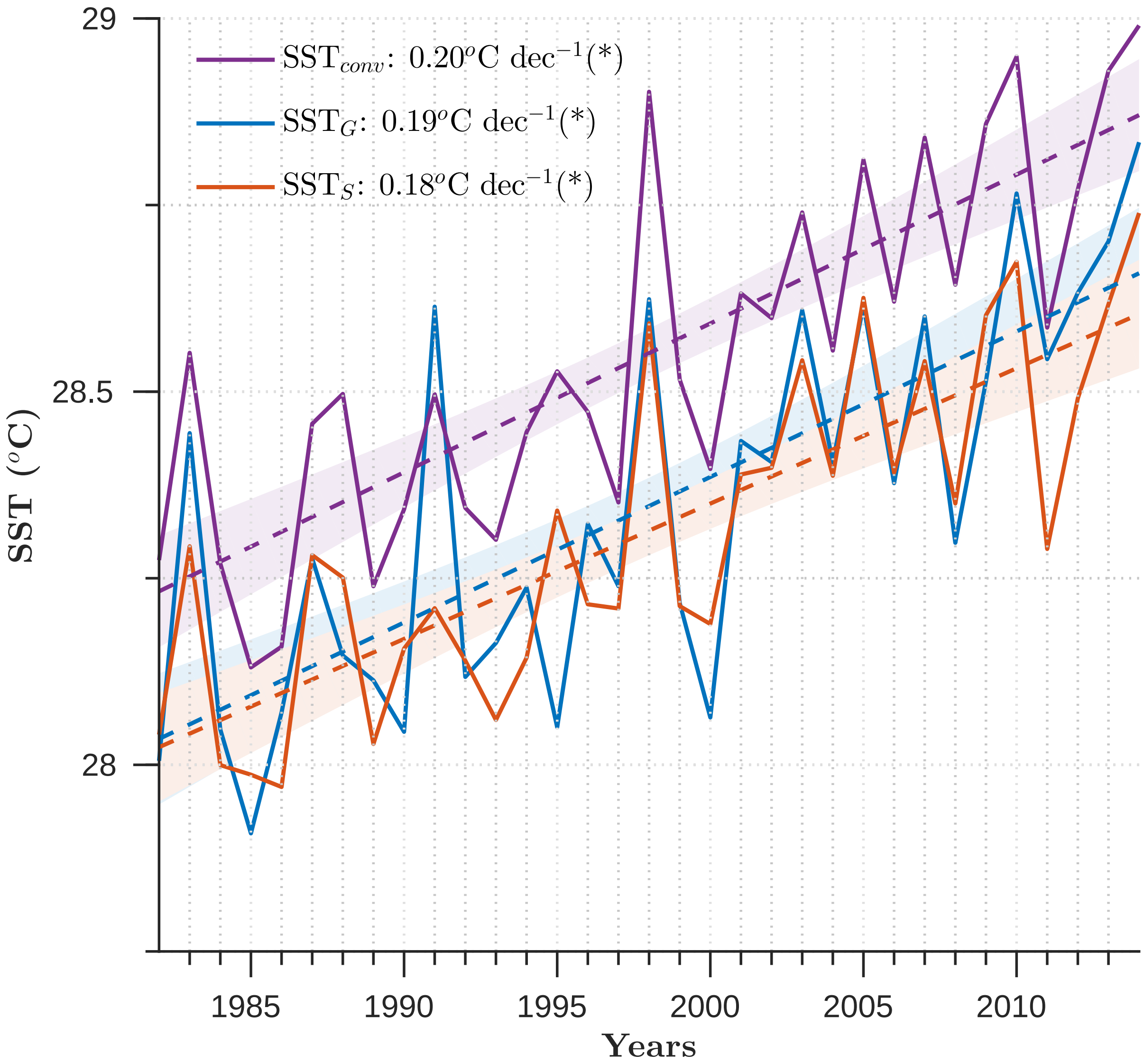


Figure 4–1: Observed time series of $SST_G$, $SST_{conv}$, and $SST_S$ in 1/4$^o$ daily NOAA/OISST, averaged over the 5 basins with the most TC activity during TC season. Annual values SST at TC genesis ($SST_G$), SST at location of deep tropical convection ($SST_{conv}$) and SST over the main development regions during TC season ($SST_S$) are shown between 1982 and 2014, with the time mean computed over the TC season. For each curve the long-term linear trend (dashed lines) and the 95% confidence interval (shaded area) are also shown. The (*) indicates that the trend is statistically significant.

The tropical atmosphere transitions from a subsaturated free-troposphere to one that is saturated and continuously convecting as TC genesis occurs. However, most deep convection events in the tropical atmosphere are not associated with TC genesis—there are approximately 5000 times more tropical deep convection events than TC genesis events with the $1^o$ horizontal resolution OLR dataset. It is, therefore, of interest to compare the trend in SST during all deep convection events to that of $SST_G$ to see if the trends differ for these more extreme events. $SST_G$ and $SST_{conv}$ have comparable trends which are slightly greater than the long-term trend in TC season-mean SST of 0.18 $^o$C decade$^{-1}$ (Fig. 4–1). The mean values of $SST_G$ and $SST_{conv}$ are similar (28.5$^o$C), with $SST_{conv}$ actually slightly warmer than $SST_G$ because TC genesis generally occurs poleward of the region of most frequent deep convection (*Berry and Reeder*, 2014).

Table 4–1 shows the values of the trends in $SST_G$, $SST_S$, and $SST_{conv}$ for each ocean basin. These trends are significant for most of the individual ocean basins and the magnitude of the warming trend at time of TC genesis or deep convection is typically comparable to the seasonal-mean warming trend in the MDR ($SST_S$). However, SST in isolation does not determine whether there is convection because upper-tropospheric temperature also affects convective stability of the atmosphere. The upper-troposphere anomalies are linked to changes in the tropical-mean SST (*Sobel et al.*, 2002) or the SST changes in regions of deep convection (*Flannaghan et al.*, 2014). The warming of upper-tropospheric temperatures due to the remote effect of SST changes imply that, in some basins, the trend in $SST_{conv}$ and $SST_G$ may be stronger than the trend in $SST_S$ to meet the conditions for convection or TC genesis, as the East Pacific illustrates (Table 4–1).

These SST trends have implications for environmental conditions that affect aspects of TC activity. Tropical cyclone rainfall is strongly influenced by SST because near-surface air temperature is tightly coupled to it and this, in turn, affects the water vapor content via the Clausius-Clapeyron relation (*Trenberth et al.*, 2007; *Knutson et al.*, 2010). The warming of $SST_G$ implies a 2-3.5% increase in TC rainfall at genesis over the last three decades, provided other factors that affect rainfall, such as storm structure, have not changed. Furthermore, maximum tropical cyclone intensity depends on the air-sea

Table 4–1: Linear trends of annual-mean $SST_G^{track}$, $SST_G^{env}$, $SST_G$, $SST_{conv}$, and $SST_S$, and the coefficient of correlation (CC) between $SST_G$ and $SST_S$ time series for each ocean basin. The trends (in $^o$C decade$^{-1}$) and the 95% two-sided confidence interval are calculated for the period 1982-2014 for each basin. The star indicates that the trend is statistically significant at the 5% level.

| **Basin** | $\mathbf{SST}_G^{track}$ | $\mathbf{SST}_G^{env}$ | $\mathbf{SST}_G$ | $\mathbf{SST}_S$ | **CC** | $\mathbf{SST}_{conv}$ |
|---|---|---|---|---|---|---|
| NA | -0.01 ± 0.14 | 0.25* ± 0.10 | 0.27* ± 0.15 | 0.27* ± 0.06 | 0.56 | 0.31* ± 0.07 |
| WP | -0.02 ± 0.07 | 0.21* ± 0.06 | 0.20* ± 0.07 | 0.21* ± 0.06 | 0.7 | 0.21* ± 0.06 |
| EP | 0.04 ± 0.10 | 0.16* ± 0.07 | 0.23* ± 0.13 | 0.06 ± 0.12 | 0.18 | 0.14* ± 0.10 |
| SP | -0.13 ± 0.16 | 0.21* ± 0.16 | 0.09 ± 0.18 | 0.16* ± 0.08 | 0.42 | 0.15* ± 0.07 |
| SI | 0.01 ± 0.09 | 0.20* ± 0.10 | 0.17* ± 0.09 | 0.17* ± 0.07 | 0.53 | 0.20* ± 0.08 |
| Global | -0.03 ± 0.06 | 0.20* ± 0.03 | 0.18* ± 0.07 | 0.18* ± 0.04 | 0.82 | 0.20* ± 0.04 |

enthalpy disequilibrium and the difference between near-tropopause and SST, according to potential intensity theory (*Emanuel*, 2003). Recent work has shown that changes in the difference between near-tropopause and SST are typically modest compared to the air-sea disequilibrium (*Wing et al.*, 2015). Though other factors like surface relative humidity also affect the air-sea disequilibrium, an increase with SST is the leading-order behavior for radiatively forced climate changes (*Emanuel*, 1987; *Emanuel and Sobel*, 2013).

SST at the time of tropical cyclone genesis is indicative of conditions in the main development regions of TCs. However, the changes in the storm-local environmental conditions can arise from both variations in the geographic distribution of storm tracks (*Kossin*, 2015) and from temporal changes in the climatological regions of TC development, which correspond to Eulerian temperature trends (*Kossin et al.*, 2014).

Figure 4–2 shows the time-series of $SST_G$ and the effect of TC track changes on SST trend ($SST_G^{track}$), which is obtained using long-term monthly-mean SST values to determine SST at location of genesis. The figure also shows the effect of environment changes only ($SST_G^{env}$) by randomizing TC genesis events between years in order to remove the influence of geographic shifts of the tracks. The trend in $SST_G^{track}$ is negative (-0.03$^o$C dec$^{-1}$), consistent with the observed poleward migration of global TC tracks (*Kossin et al.*, 2014) (Fig. B–3) toward colder regions. The trend due to environmental warming ($SST_G^{env}$) is positive (0.20$^o$ dec$^{-1}$) and close to the one observed for $SST_S$ (0.18$^o$ dec$^{-1}$).

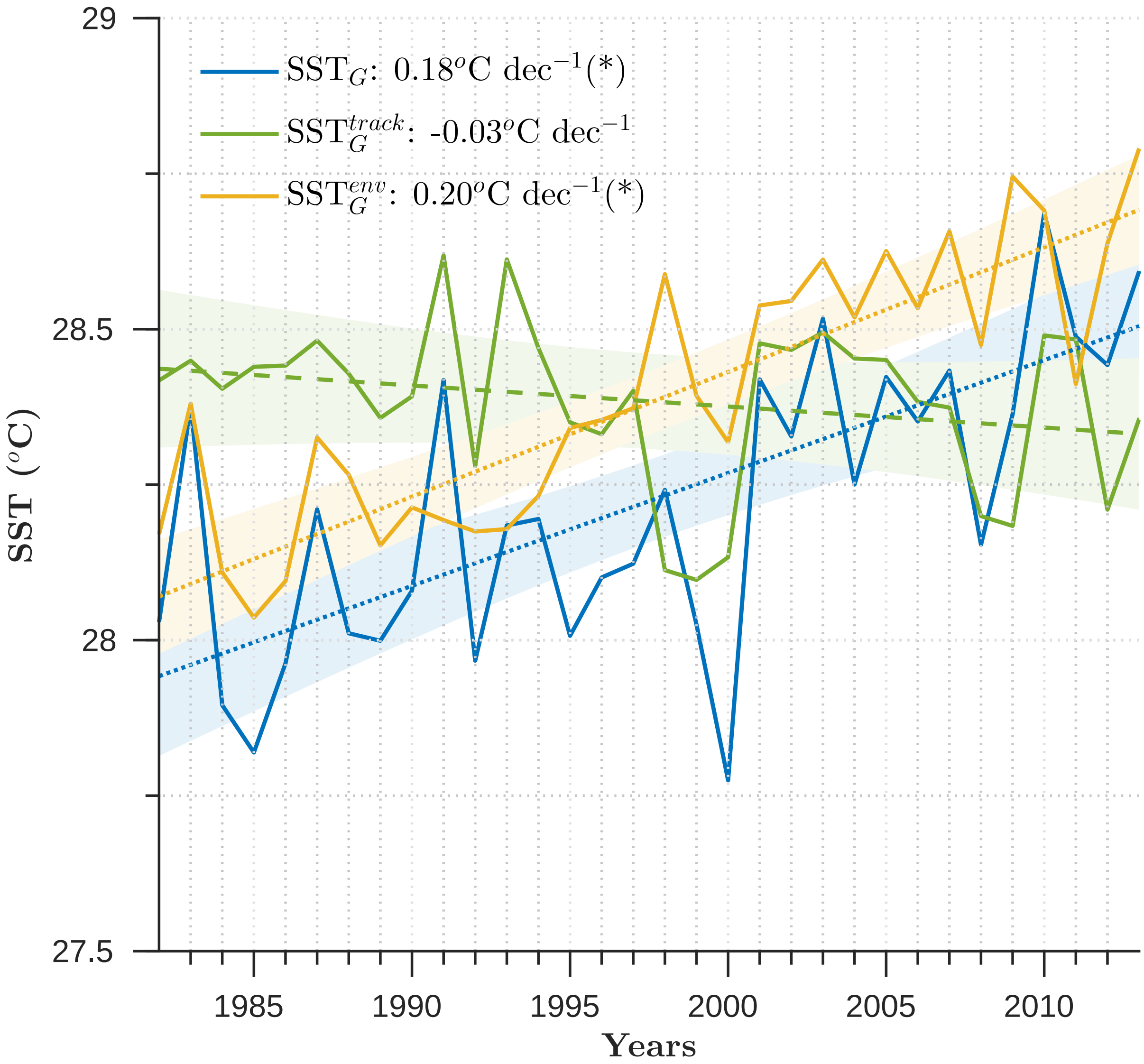


Figure 4–2: Observed time series of $SST_G$, and time series of $SST_G^{env}$ and $SST_G^{track}$, obtained with all the TCs observed between 1982 and 2014. The SST at TC genesis ($SST_G$) is compared to that arising from the temporal changes in local TC genesis environment ($SST_G^{env}$) and that arising from track migration ($SST_G^{track}$). For each curve the linear long-term trend (dashed lines) and the 95% confidence interval (shaded area) are also shown. The (*) indicates that the trend is statistically significant.

Table 4–1 shows the values of the trends in $\mathrm{SST}_G^{env}$ and $\mathrm{SST}_G^{track}$ for individual ocean basins. The trend in $\mathrm{SST}_G$ can be affected by both the trends in $\mathrm{SST}_G^{env}$ and $\mathrm{SST}_G^{track}$. Indeed, the trend in $\mathrm{SST}_G$ is slightly smaller than the trend in $\mathrm{SST}_G^{env}$ when the trend in $\mathrm{SST}_G^{track}$ is negative, as for global SSTs (Figure 4–2) and somewhat greater otherwise (e.g., EP and SI basins). As the trend in $\mathrm{SST}_G^{track}$ is generally small and not statistically significant, the trend from local changes in the TC season environment is generally similar to the trend in $\mathrm{SST}_G$. In the East Pacific basin, the positive effect of track changes amplifies the effect of global warming and the trend in $\mathrm{SST}_G$ is larger than the trend in $\mathrm{SST}_S$. The South Pacific, in contrast, has a cooling effect of TC track migration that offsets the increase in SST due to environmental warming such that the trend in $\mathrm{SST}_G$ is weaker than the one in $\mathrm{SST}_S$ and no longer statistically significant.

One should note that $\mathrm{SST}_G$ corresponds to an average for all TCs that occurred over the different ocean basins in a given year such that it is not directly related to global TC frequency. A change in the distribution of TC events between the ocean basins, such as an increase in frequency in the climatologically warm ocean basins, could affect $\mathrm{SST}_G$. However, this would appear as a trend in $\mathrm{SST}_G^{track}$, which Figure 4–2 shows is not significant.

It is of interest to examine if the conclusions drawn with observed TC tracks hold with tracks obtained from TC-permitting climate model simulations that are used for projections of future TC activity. Here we examine the TC tracks simulated by the High Resolution Atmospheric Model (HiRAM). This model has been developed by NOAA's Geophysical Fluid Dynamics Laboratory and, when forced with observed SST boundary condition, is able to reproduce well several aspects of the tropical cyclone frequency variability observed for the past three decades (*Zhao et al.*, 2009; *Shaevitz et al.*, 2014).

Figure 4–3 shows the time series of $\mathrm{SST}_G$ computed using all the TC tracks from IBTrACS (observed) and 3 ensemble members of HiRAM simulations using HadISST for the lower boundary condition over the period between 1980 and 2008. The mean $\mathrm{SST}_G$ values obtained with the simulated TC tracks are colder than those obtained from

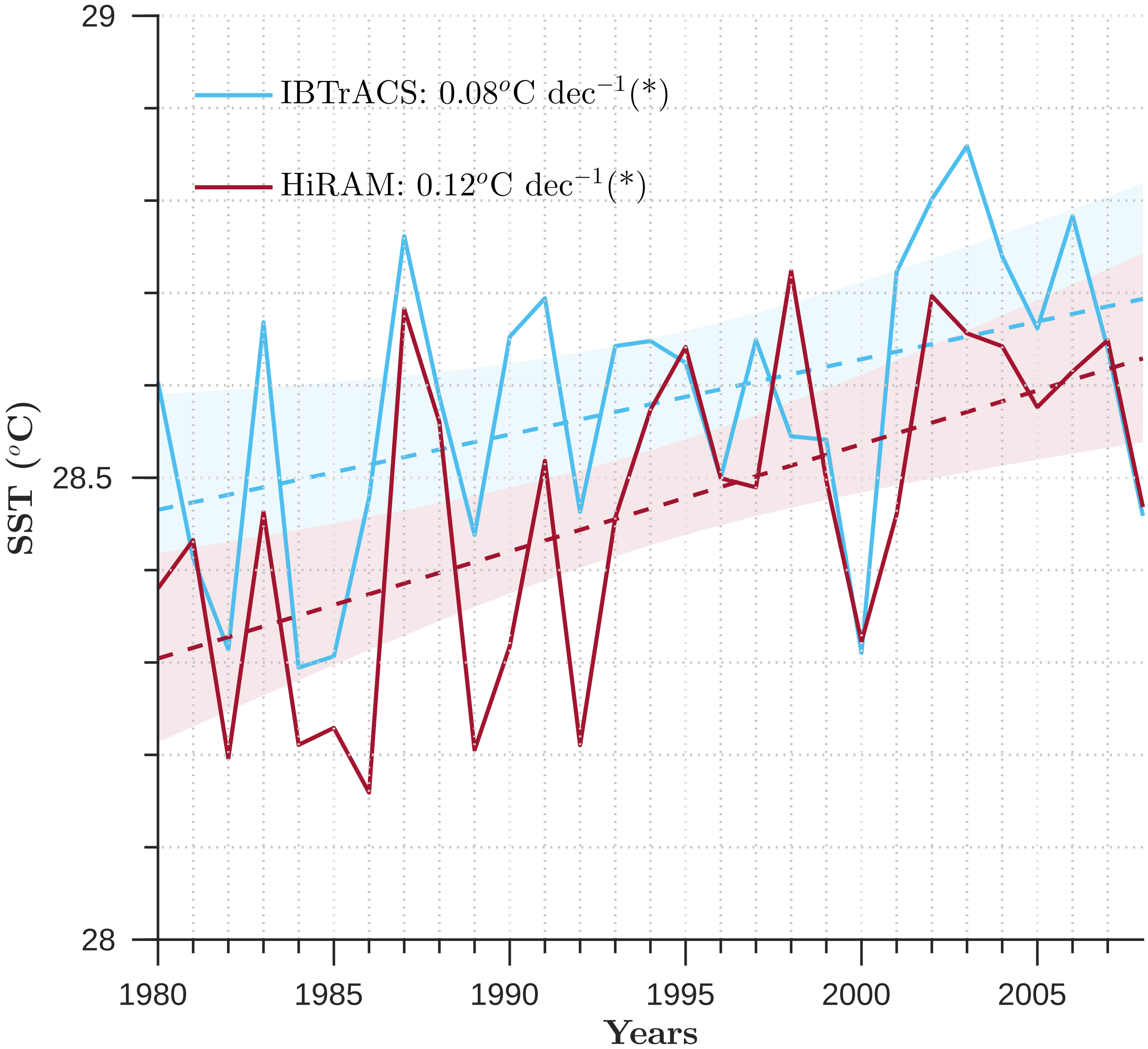


Figure 4–3: Time series of SST$_G$ obtained with IBTrACS (observed) and HiRAM (simulated) TC tracks. The SSTs at TC genesis (SST$_G$) are determined for all the TCs observed between 1980 and 2008 using IBTrACS data and for all the TCs simulated by three HiRAM realizations over the same period. The TC tracks are combined with HadISST monthly data. For each curve the linear long-term trend (dashed lines) and the 95% confidence interval (shaded area) are also shown. The (*) indicates that the trend is statistically significant.

observations. This arises from a zonal shift in some of the main development regions in HiRAM toward climatologically colder regions.

The observed long-term trend in $SST_G$ in HadISST of $0.08^o$ dec$^{-1}$ is smaller than that obtained with HiRAM simulated tracks ($0.12^o$ dec$^{-1}$). The weaker trend in $SST_G$ computed using IBTrACS dataset of TC tracks likely comes from the observed global poleward track migration of approximately $0.76^o$ dec$^{-1}$ over this time period (Fig. B–4). A poleward track migration weakens the trend in $SST_G$, as previously noted. The tracks simulated by HiRAM show a smaller, non-significant poleward trend ($0.11^o$ dec$^{-1}$, Fig. B–3) such that the corresponding $SST_G$ trend almost exclusively arises from the local environmental warming. Therefore, the magnitude of the long-term warming trend with HiRAM-simulated TC tracks is larger than the observed, IBTrACS trend.

SST at TC genesis has significantly increased over the last three decades, and this reflects the mean warming trend of the main development regions of TCs during the TC season. Warming tropical ocean surface temperatures over this time period has been attributed to anthropogenic radiative forcing. The observed warming trend in SST at TC genesis is primarily due to the temporal changes of the basins' SST, which is slightly counterbalanced by the poleward migration of TC tracks to climatologically colder regions. We note that while the warming trend is significant across available SST datasets, its magnitude varies substantially and there is a need to reconcile the differences between observational SST estimates.

## 4.1 Methods

### 4.1.1 Data

The $1/4^o$ daily Optimum Interpolation Sea Surface Temperature (OISST) dataset (*Reynolds et al.*, 2007) from the National Oceanic and Atmospheric Administration (NOAA) provides daily mean values of SST with a horizontal resolution of $0.25^o$ from 1982 to the present.

The Outgoing Longwave Radiation (OLR) data come from NOAAs Climate Data Record (CDR) Program, version 1.2 (*Lee*, 2014). The OLR daily values are given with a $1^o$x$1^o$spatial resolution and are available from 1979 to 2014.

The release v03r08 from the International Best Track Archive for Climate Stewardship (IBTrACS) (*Knapp et al.*, 2010) provides information, such as position and wind speed, every 6 hours of all the tropical storms from 1842 to 2014.

The HiRAM TC tracks simulated in the Coupled Model Intercomparison Phase 5 (CMIP5) AMIP experiment are combined with the Met Office Hadley Centre's sea surface temperature dataset (HadISST (*Rayner et al.*, 2003)), which was used for the simulation's prescribed SST boundary condition. The HadISST dataset provides monthly mean SST values with a horizontal definition of $1^o$x $1^o$.

### 4.1.2 Methodology

The present study focuses on the long-term trends in SST at tropical cyclone genesis and for all the tropical convection events, over the 33-year period from 1982 to 2014. Consistent with previous studies (*Dare and McBride*, 2011; *Tory and Dare*, 2015), we refer to tropical cyclones (TC) as the storms that satisfy the 3 following conditions: 1. the maximum sustained wind reaches 18 m $s^{-1}$ at one point, which defines the *genesis* of the tropical cyclone, 2. the storm is labeled as "tropical" in the IBTrACS database, and 3. the latitude at genesis is equatorward of $35^o$ latitude.

The SST at the time of genesis is obtained by linear interpolation in time between OISST daily means (or HadISST monthly means) to the time of genesis. We also averaged meridionally the SST over $1.5^o$ of latitude (*McTaggart-Cowan et al.*, 2015).

The five basins with the most TC activity are examined here: North Atlantic, West Pacific, East Pacific, South Pacific, and South Indian and the sea surface temperature of each basin during its TC season (referred as $SST_S$) is also examined. The spatial extent and the months defining the TC season of each basin correspond to the main development region and period as shown in Table B–1.

Note Figure 4–1 only includes the TCs in the spatial and temporal definition of the basin's TC season, to be consistent with deep convection events examined. In the other figures and Table 4–1, all the TCs that occurred in the given basins are included.

The variations in $SST_G$ over the analysis period are decomposed between the part due to the environmental warming and the part due to track changes, respectively referred as $\mathrm{SST}_G^{env}$ and $\mathrm{SST}_G^{track}$. The values of $\mathrm{SST}_G^{env}$ are obtained by assigning a random year of genesis to the tropical cyclones, keeping the location, the day, and the month of genesis unchanged. For a given year, this process shuffles the location of genesis and thus removes the effect of systematic track migration. We repeated this process 100 times and averaged over the 100 realizations to obtain a robust value of $\mathrm{SST}_G^{env}$.

The values of $\mathrm{SST}_G^{track}$ are obtained at the location and month of each TC genesis event, using long-term monthly-mean values of SST. The long-term means are calculated for each horizontal grid point and each month by averaging over the 1982-2014 period. The trends in $\mathrm{SST}_G^{track}$ include the effect of the migration of TC tracks to climatologically colder or warmer regions.

In addition to the tropical cyclones that are extreme events, we considered all the events of tropical deep convection that occurred over the same time period. We considered OLR values smaller than 240 $\mathrm{Wm}^{-2}$ to be convection events (*Graham and Barnett*, 1987). The tropical deep convection events that occurred over the five basins of interest (NA, WP, EP, SP, SI) during TC season, between 1982 and 2014, are considered. Here we used the same spatial and seasonal definitions of the TC season of the basins (Table B–1). We examined SST at the location where there is deep convection for all these events (referred as $\mathrm{SST}_{conv}$).

The time series shown correspond to annual values for each year's TC season and the trends are obtained by linear regression. The determination of the 95% confidence interval and the statistical significance of the trend—i.e., the rejection of the null hypothesis of no trend at the 5% level—take into account autocorrelation of the time series (*Wing et al.*, 2015; *Santer et al.*, 2000).

### 4.2 Acknowledgments

We acknowledge NOAA for providing the daily Optimum Interpolation Sea Surface Temperature dataset (https://www.ncdc.noaa.gov/oisst), the IBTrACS database (http://www.ncdc.noaa.gov/ibtracs), and Interpolated Outgoing Longwave Radiation daily values (http://www.esrl.noaa.gov/psd/data/gridded/data.olrcdr.interp.html). We also thank

Ming Zhao (Geophysical Fluid Dynamics Laboratory) for providing storm tracks from CMIP5 AMIP experiments with HiRAM-C180. We sincerely acknowledge the support of Stephen and Anastasia Mysak Graduate Fellowship (C.D.) and the support of NSERC Discovery Grant (T.M.).

## Connecting text: Chapter 4 and Chapter 5

Chapters 3 and 4 present analyses of the observed SST distribution and long-term trends, suggesting that SST at TC genesis reflects SST observed in summer environment. Consequently, SST seems not to be a good predictor for TC genesis within the main development regions. However, the newly observed warming trends in SST at TC genesis that are mainly due to warming of the tropical SST and, to a smaller extent, to the migration of TC tracks, can have important implications for some aspects of tropical cyclone activity, such as intensity and rainfall.

The observed trends in SST at the time of TC genesis differ across the ocean basins; for instance it is stronger in the North Atlantic basin than in the Pacific. Therefore, it is of interest to understand how zonally asymmetric warming may affect tropical cyclone genesis. This question is examined in Chapter 5 using idealized simulations with prescribed zonally asymmetric boundary conditions, as a simple way of representing different ocean basins.

# CHAPTER 5
# Response of tropical cyclone frequency to zonally asymmetric conditions in idealized climate model simulations

## 5.1 Introduction

Local variations of environmental parameters may affect tropical cyclone activity. For instance, tropical cyclone frequency in North Atlantic is slightly more strongly correlated to relative SST—define as the difference between the SST in the tropical Atlantic main development region and the tropical mean SST—than to absolute SST (*Vecchi et al.*, 2008). However, previous studies showed that absolute or relative sea surface temperature alone are not good environmental predictors for TC genesis and other factors, such as wind speeds and surface energy fluxes may also need to be taken into account (*Emanuel*, 2003). Furthermore, the latitude of the Inter Tropical Convergence Zone (ITCZ) also affects TC frequency; if a poleward shift occurs under warmer climate, this can lead to an increase in TC frequency (*Merlis et al.*, 2013). Contemporary theories for ITCZ location posit a central role for atmospheric energy transport (*Kang et al.*, 2009); rather than SST (*Kang and Held*, 2012).

It is of interest to examine how regional changes in environmental parameters may affect storm activity and which variables are dominant in determining TC frequency. Here we use an atmospheric general circulation model (GCM) with zonally asymmetric ocean fluxes in a slab-ocean surface boundary conditions to analyze how the environmental variables and the tropical cyclone frequency respond to such conditions.

## 5.2 Model description

### 5.2.1 Aquaplanet GCM

The model used is the High Resolution Atmospheric Model (HiRAM) developed by the Geophysical Fluid Dynamics Laboratory of the National Oceanic and Atmospheric Administration (NOAA) in aquaplanet simulations with Earth-like insolation (solar constant $S_0$ = 1400 W m$^{-2}$). The general circulation model (GCM) has 50-km horizontal resolution and 32 vertical levels. The slab-ocean surface boundary condition has the heat capacity of 20 m of water and accounts for radiative and turbulent surface fluxes to determine the surface temperature in an energetically consistent fashion. In HiRAM simulations forced with comprehensive boundary conditions and observed SSTs, the climatological cycle of tropical cycle frequency is well simulated (*Zhao et al.*, 2009), though the 50-km resolution is not adequate to capture the most intense TCs.

Here we present simulations with a reference $CO_2$ concentration of 300 ppm and perturbation simulations with 4 x $CO_2$ concentration and idealized energy sources and sinks in the slab ocean boundary condition that represent the ocean heat flux convergence. This is the only aspect of the forcing and boundary conditions that breaks zonal symmetry (Chapter 5.2.2).

The symmetry between the hemispheres is broken by a cross-equatorial ocean heat flux $\mathbf{F}$, leading to the Northern Hemisphere (NH) summer-season conditions. The heating (or cooling) that causes the flux $\mathbf{F}$ is $Q = -\nabla \cdot \mathbf{F}$ given by the equation 5.1 following *Kang et al.* (2008), where $\phi$ is latitude.

$$Q = \begin{cases} -Q_0 * \sin(\frac{\phi+90-w_0}{w_0}\pi) & for \ -90 < \phi < -(90-w_0) \\ -Q_0 * \sin(\frac{\phi-(90-w_0)}{w_0}\pi) & for \ 90-w_0 < \phi < 90 \\ 0 & otherwise \end{cases} \tag{5.1}$$

The prescribed cross-equatorial heat flux converges in the northern extratropics ($Q < 0$) and diverges in the southern extratropics ($Q > 0$), as shown on the right panel of Figure 5–1. Positive values of Q-flux correspond to divergent fluxes and thus to a cooling tendency, consequently the northern hemisphere is warmer than the southern one. This forcing has a zero global mean, so it does not add or subtract energy from the global system. Prescribing energy fluxes rather than surface temperatures avoids nonphysical surface fluxes that may occur with specified SST distribution.

The values of $Q_0$ and $w_0$ are set to 40 W $m^{-2}$ and 50° respectively, which result in Earth-like zonal-mean temperature and precipitation. This implies a cross equatorial ocean energy flux that is approximately twice as large as the one observed. In these conditions the inter-tropical convergence zone (ITCZ) is located at approximately 8° N

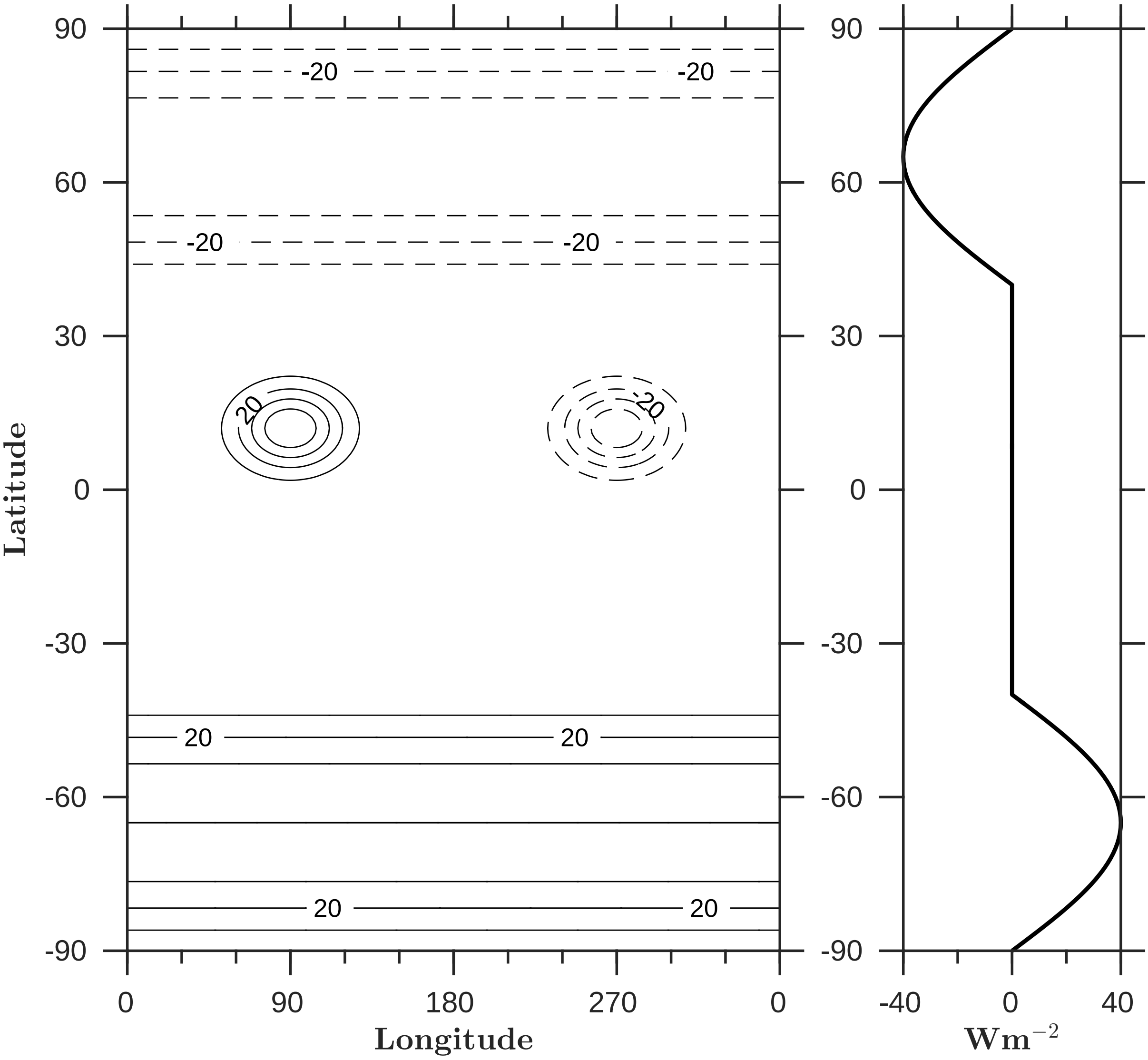


Figure 5–1: Ocean energy flux divergence, Q-flux, for which positive values correspond to cooling tendency. (left) Contours of Q-flux at surface with contour intervals of 20 W m$^{-2}$ and negative values are dashed. (right) Latitude vs zonal-mean Q-flux.

for 1 x $CO_2$ and 12° N for 4 x $CO_2$, consistent with previous results with zonally symmetric forcing and boundary conditions (*Merlis et al.*, 2013).

### 5.2.2 Zonal asymmetry

In order to study the impact of East-West contrasts on tropical cyclone genesis, the zonally symmetric Q-flux described above is perturbed by two Gaussian lobes:

$$Q' = \pm A_{asym} * \exp\left[-\frac{(\lambda-\lambda_0)^2}{\sigma_x^2} - \frac{(\phi-\phi_0)^2}{\sigma_y^2}\right], \tag{5.2}$$

where $\lambda$ is longitude, $\phi_0 = 12°$, $\sigma_x = 30°$, and $\sigma_y = 8°$ are the longitudinal and meridional extent of the anomalies. To ensure that the anomalies cancel each other in a zonal mean so that there is no energy added to the system, a positive anomaly is added at $\lambda_0 = 90°$ and a negative anomaly is added at $\lambda_0 = 270°$. The two are located at the same latitude ($\phi_0 = 12°$) and have the same meridional extent ($\sigma_y = 8°$). These values correspond to the latitude of the ITCZ and the approximate meridional width of the area where the rate of precipitation is higher than 8 mm day$^{-1}$ on each side of the maximum precipitation, such that the anomalies are within the region of active convection.

Figure 5–1 shows the longitude-latitude contours of the prescribed Q-flux and its zonal mean, which corresponds to Q given by the sum of equation 5.1 and equation 5.2. This prescribed heat flux acts to cool the region around 90°E and warm the region centered in 270°E. We have performed simulations with different values of $A_{asym}$ between 50 and 150 W m$^{-2}$.

One can think of the climatologically warm tropical region near 270° as analogous to the tropical West Pacific "warm pool" and the climatologically cold tropical region near 90° as analogous to the Atlantic or East Pacific. We note that having the warm region in the eastern part of the domain is different from Earth's climate; however, the convention for longitude is arbitrary in aquaplanet simulations.

### 5.2.3 Temporal evolution of the simulations

In order to determine the time of convergence to a statistically steady state, a simulation has been run for 20 years and the zonal-mean profiles of temperature and precipitation have been examined. Both profiles take between 5 and 10 years to reach a quasi-stable state. For the results that follow, the simulations have been run for 20 years and the results are averaged over the last 10 years.

### 5.2.4 List of the simulations

Table 5–1 enumerates all the simulations that have been run and that are examined hereafter.

Table 5–1: List of the simulations.

| $CO_2$ (ppm) | $A_{asym}$ (W $m^{-2}$) |
|---|---|
| 300 | 0 |
| | 50 |
| | 100 |
| | 150 |
| 1200 | 0 |
| | 50 |
| | 100 |
| | 150 |

### 5.3 Response to zonally asymmetric conditions in SST and precipitation

Prescribing asymmetric conditions through an oceanic energy flux directly affects SSTs as a net positive Q-flux corresponds to a cooling tendency and thus to a cold region. The analysis of precipitation rates in simulations with zonally asymmetric Q-flux gives an indication of the response of deep convection to these energy and SST conditions.

Figure 5–2 shows the relative changes in SST, precipitation, and latitude of ITCZ for simulations with the zonally asymmetric part of the Q-flux (Q'), with respect to the zonally symmetric simulation with the same $CO_2$ concentration. Here the amplitude of Q' is set to $A_{asym}$ = 150 W $m^{-2}$ with both 1 x $CO_2$ and 4 x $CO_2$. The changes in SST and precipitation are shown for the region of asymmetric forcing, meridionally averaged between 4°N and 20°N. The absolute values of these three environmental variables are given in Appendix C. The anomalies in SST and precipitation rate are negatively correlated with Q': both increase where Q' is negative and decrease where it is positive. This is consistent with the facts that positive Q-flux correspond to a cooling tendency and that warm SSTs favor deep convection. There are also small opposite anomalies to the north and south of the forcing regions. The location of the ITCZ, defined as the latitude where the precipitation rate is maximal, is no longer zonally uniform when Q' is added; it shifts a few degrees poleward in the warm region and equatorward in the cold region.

Figure 5–2 shows that increasing the $CO_2$ concentration tends to damp the effect of the zonal asymmetry on these three aspects of the simulated climate. The location of the ITCZ shifts poleward in the zonal mean when the $CO_2$ concentration is quadrupled and the local migrations of the ITCZ over the warm and cold regions are damped. When

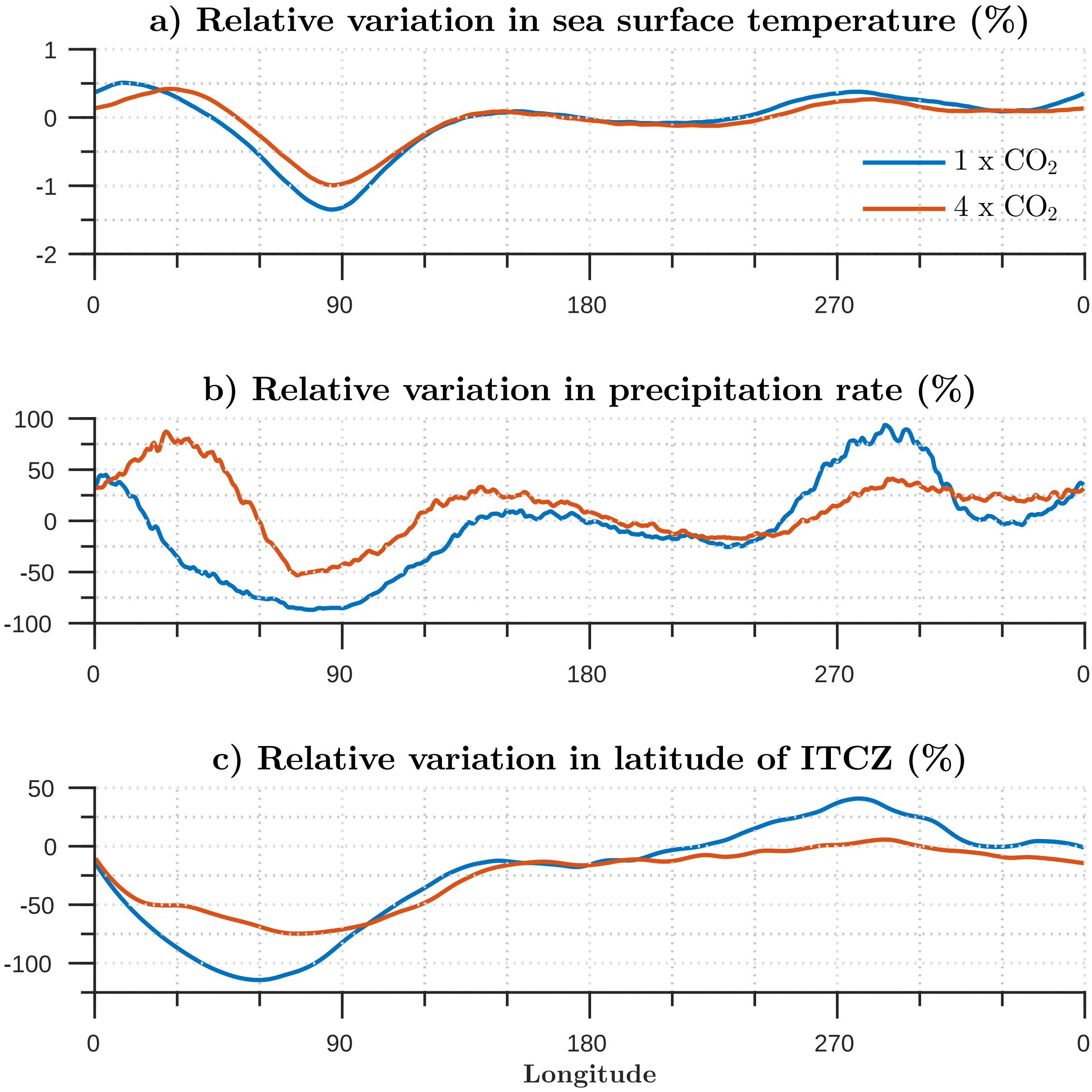


Figure 5–2: Relative changes in (a) sea surface temperature, (b) precipitation and (c) the latitude of ITCZ due to the zonally asymmetric part of the Q-flux, Q', for 1 x $CO_2$ and 4 x $CO_2$, in the region of forcing vs longitude. $A_{asym}$ is set to 150 W m$^{-2}$ and the changes are meridionally averaged between 4°N and 20°N. Figure C–1 shows the full fields.

the $CO_2$ concentration is quadrupled in the zonally symmetric case, the global-mean SST increases by 4.8°C, the global-mean precipitation rate increases by 0.3 mm day$^{-1}$ and the ITCZ latitude shifts poleward by 4.3°. When the climate is zonally asymmetric, the response of global-mean temperature and zonal-mean ITCZ latitude to an increase in $CO_2$ is less sensitive. The global-mean temperature in the 4 x $CO_2$ simulation is warmer by 4.6°C and the ITCZ is more poleward by 3.1° latitude than in the corresponding 1 x $CO_2$ simulation, for $A_{asym}$ = 150 W m$^{-2}$.

Different values for $A_{asym}$ and $w_{asym}$ have been tested in order to assess the sensitivity of climate variables to these parameters. Generally the anomalies in SST and precipitation reflect well the prescribed Q-flux, in particular in terms of amplitude and width. Similarly, the shift of the ITCZ with respect to the symmetric simulations is larger when $A_{asym}$ increases. Furthermore, increasing $A_{asym}$ tends to amplify the differences in responses magnitude between the warm and the cold regions. For all variables the positive anomaly is weaker than the negative one. The negative anomaly in precipitation and latitude of ITCZ expands more westward than the SST anomaly, which is not the case for the positive anomalies. This phenomenon is more marked for 1 x $CO_2$ than for 4 x $CO_2$. The global-mean SST and precipitation rate are nearly unchanged whereas the ITCZ globally shifts poleward when the climate state is zonally asymmetric, consistent with *Shaw et al.* (2015).

Figure 5–3 shows the surface energy fluxes vs longitude averaged between 4°N and 20°N. The decomposition of the surface energy budget helps explaining the dissimilarity of the responses between the cold and the warm regions. The main difference between these two regions, aside from the Q-flux, comes from the latent energy (LE) fluxes, counterbalanced by the shortwave (SW) radiative fluxes. The anomalies in sensible heat (SH) fluxes over regions of positive and negative Q' are of the same amplitude with opposed signs and do not help explaining the different responses between these regions. In zonally asymmetric simulations, the structure of surface relative humidity helps explaining that the zonal asymmetry in surface temperature needed to give the required amount of latent surface flux is bigger in the cold region (less subsaturated) than in the warm region (more subsaturated, see Figure C–2).

In the cold region where Q' is positive (90°E), the reduction of the latent heat fluxes is counterbalanced by an increase in the absorbed radiative energy and the heat flux divergence. The response of clouds may account for the large increase in absorbed radiative energy: the decrease in the total cloud amounts, in a region that is cloudy in the absence of Q', leads to a large decrease of the planetary albedo such that the net radiative fluxes are more positive for shortwave and less negative for longwave (LW). The total net radiative fluxes are dominated by SW fluxes such that there are increased in the region of positive Q'. In contrast, the region of negative Q' is already cloudy in zonally symmetric simulations so the greater cloud amounts do not change the planetary albedo substantially and the surface radiative budget is weakly decreased over this region.

In the simulation with 4 x $CO_2$, the surface energy fluxes are slightly different from those shown in Figure 5–3. At each latitude, there is less energy loss from LW radiation, consistent with amplified greenhouse effect, and slightly weaker SH fluxes. These changes are counterbalanced by less energy absorbed by SW radiation and stronger LE fluxes. These differences between 4 x $CO_2$ and 1 x $CO_2$ simulations are similar at all the latitudes, except over the cold, cloudy tropical region near 90°E, where there is substantially less absorbed SW radiation and weaker LE fluxes in the 4 x $CO_2$ simulation than with 1 x $CO_2$. Consequently, the zonal asymmetry in SW surface fluxes decreases in the 4 x $CO_2$ simulation, consistent with the zonal asymmetry in SST and precipitation rate (Fig. 5–2).

## 5.4 Response to zonally asymmetric conditions in tropical cyclone frequency

### 5.4.1 Introduction

The tropical cyclones refer to the storms for which the maximum sustained wind speed (MSW) reaches at least 15.2 m $s^{-1}$ and the genesis event is the moment when this threshold is reached for the first time. The storms are referred as hurricanes if their MSW exceeds 29.5 m $s^{-1}$, this threshold being smaller than the usual value of 33 m $s^{-1}$ to account for the limited horizontal resolution of the model (*Walsh et al.*, 2007).

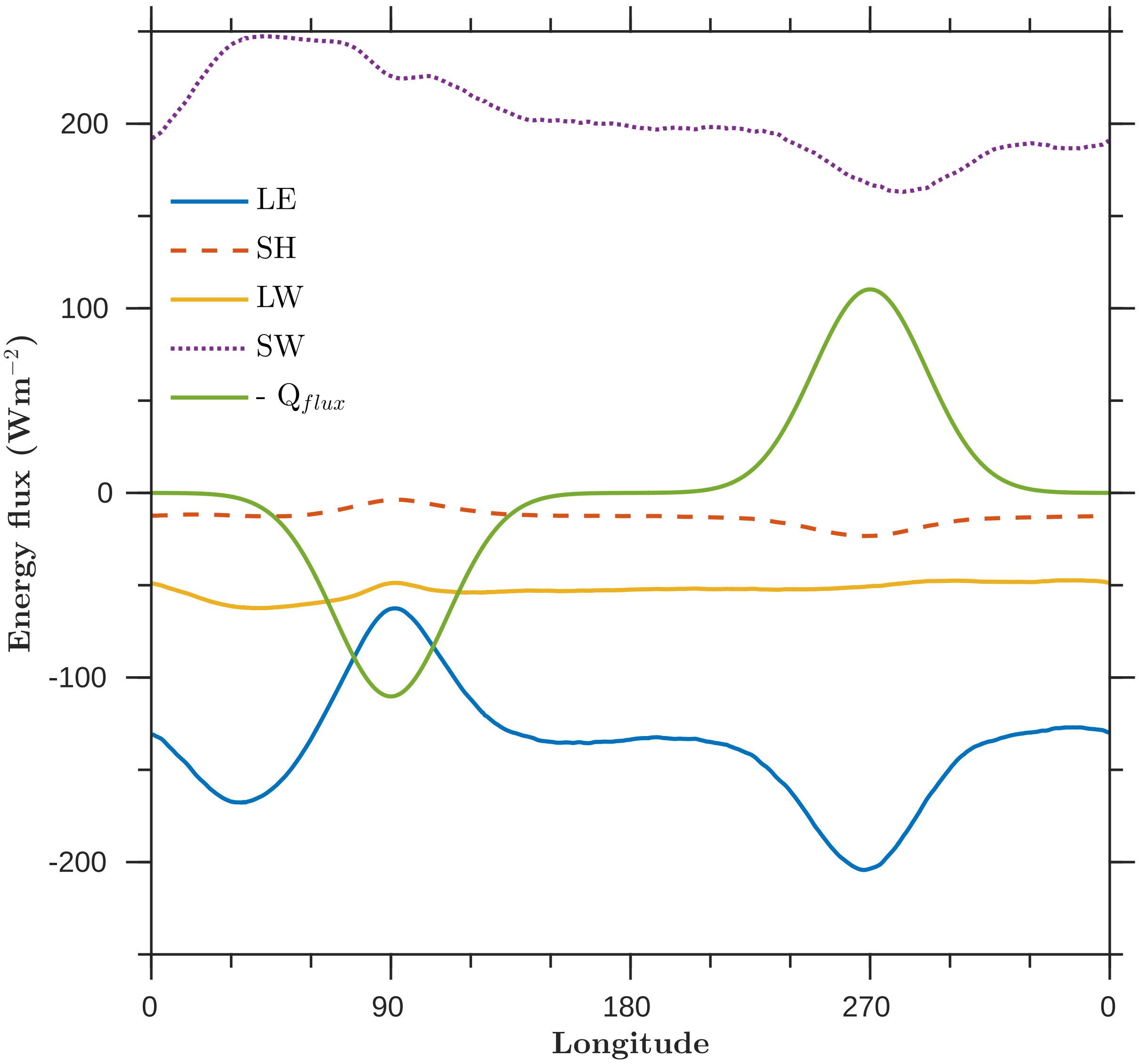


Figure 5–3: Surface energy fluxes vs longitude for the simulation with 1 x $CO_2$ and $A_{asym}$ = 150 W $m^2$. The fluxes are averaged between 4°N and 20°N.

Tropical cyclones and hurricanes are rare events and the mean rate of genesis for TCs and hurricanes (hereafter referred as $G_{TC}$ and $G_H$ respectively) are approximately 345 TCs and 26 hurricanes per year, when averaged over the 10 last years of simulation in the reference case with zonally symmetric Q-flux ($A_{asym} = 0$). In order to assess the effect of zonally asymmetric conditions on storm genesis, the simulated Earth is divided in slices of a certain longitudinal extent, w, and the number of storms that developed in each slice is averaged over 10 years. The longitude bounds of the bins are arbitrary and may impact the results, so we chose to systematically vary the bounds by shifting them to start at every 0.5° longitude.

Even for zonally symmetric Q-flux prescribed, the tropical cyclone genesis events are not uniformly distributed in longitude and there is zonal variability in $G_{TC}$ and $G_H$ because of the limited time sampling. Therefore, we will first determine what is the "natural" level of variability in the rate of storm genesis. Subsequently, we will examine the effect of the zonally asymmetric part of the Q-flux, comparing the results of the simulations with different values of its amplitude.

### 5.4.2 Natural variability in TC number

The analysis of the zonally symmetric simulations, averaged over 10 years, showed that there are "natural" zonal variations which go up to 10% of maximum precipitation rates and 1% of SSTs. This lack of zonal symmetry reveals some biases of the model and encouraged us to assess the level of noise in tropical cyclone frequency for symmetric simulations. The knowledge of the natural variability of TC and hurricane frequency will be necessary to determine whether or not zonal asymmetries significantly affect TC frequency.

Here an analysis of the zonal variability in $G_{TC}$ and $G_H$ has been conducted using simulations in a zonally symmetric reference climate, as described in *Merlis et al.* (2013). An alternative way of characterizing variability in $G_{TC}$ and $G_H$ would have been to look at time series of different years, but this method is not pursued here. Figure 5–4 shows the hurricane tracks for this reference simulation in the top panel. The tracks are spread

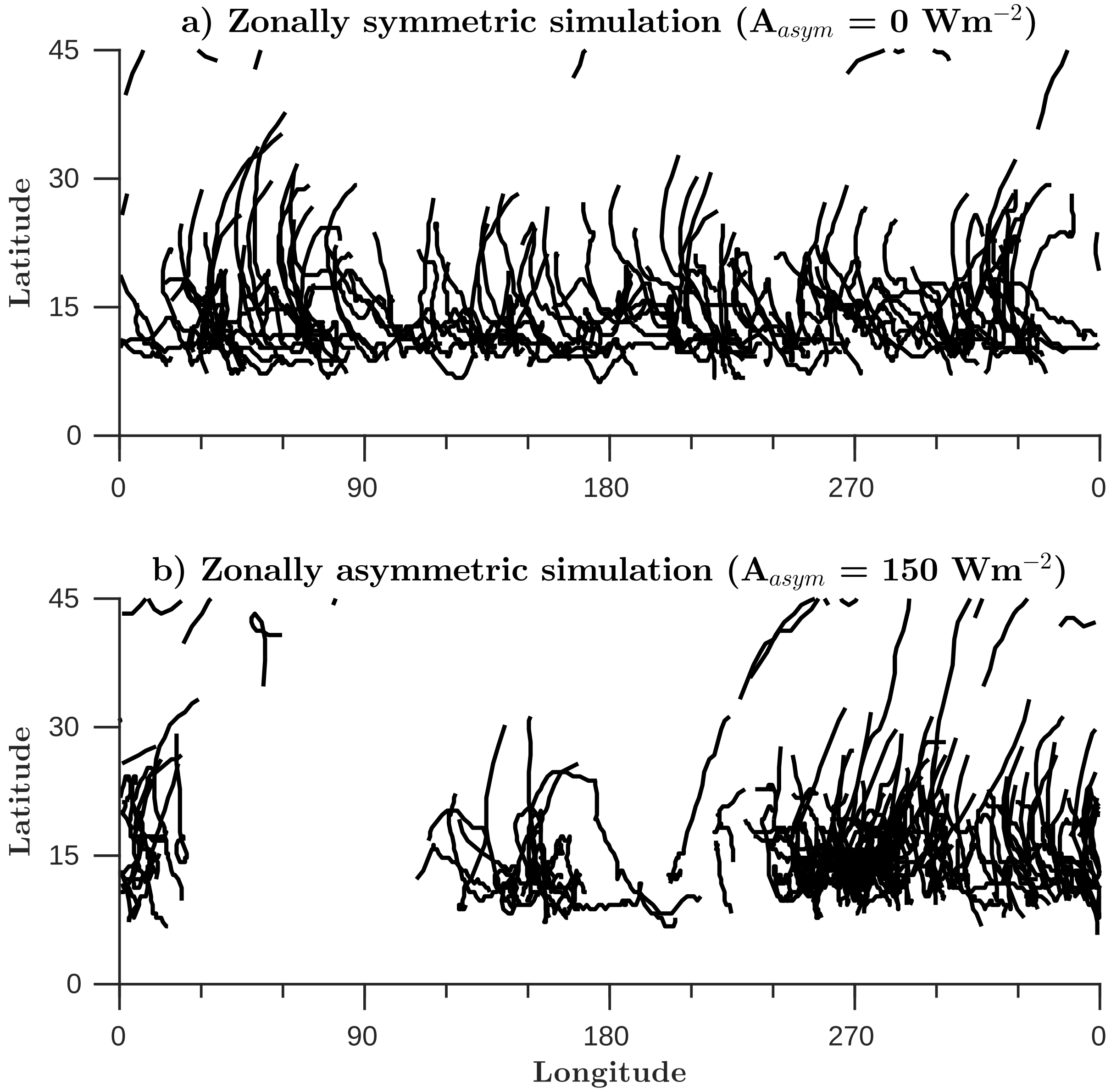


Figure 5–4: Hurricane tracks for the 5 last years of simulation with 1 x $CO_2$ and (a) $A_{asym}$ = 0 W $m^2$ (reference simulation) and (b) $A_{asym}$ = 150 W $m^2$.

over the entire longitudinal extent but there are some variations locally such that the genesis rate is not perfectly zonally homogeneous.

For different values of the longitudinal width of averaging, w, the distribution of the genesis rate G is computed. The two statistics that are of interest here are the standard deviation (SD) and the coefficient of variation (CV):

$$\begin{aligned} SD &= \sqrt{\tfrac{1}{G-1}\sum(G_i - \overline{G})^2} \\ CV &= \tfrac{SD}{\overline{G}} * 100 \end{aligned} \tag{5.3}$$

where $G_i$ is the number of TCs or hurricanes in the slice $i$ and $\overline{G}$ the globally averaged rate of genesis.

The coefficient of variation is normalized by the mean value, therefore it is a standardized measure of the extent of variability of the studied statistics with respect to the mean of the population and is the most relevant statistic for this study. The profile of CV shows a rapid decrease with the width of the bin until 25° longitude and is nearly stable for larger w.

Generally the values of CV are relatively high, suggesting that storm genesis is not perfectly zonally symmetric and that the distribution of the location of genesis events is noisy. Consequently the value of w chosen for following analysis must be large enough to reduce the CV but not too large to encompass the zonal anomalies. For a width of integration of 30° the CV is approximately 4.5% for TCs and 20% for hurricanes, for both 1 x $CO_2$ and 4 x $CO_2$ concentration, so this value of w is a good compromise and will be used hereafter.

### 5.4.3 Response in genesis frequency under zonally asymmetric conditions

Different simulations with increasing amplitude of Q' have been run with 1 x $CO_2$ and 4 x $CO_2$ concentration. In each case the longitudinal profile of $G_{TC}$ and $G_H$ have been computed. Figure 5–5 shows the relative changes in genesis rate of tropical cyclones between the zonally asymmetric and symmetric simulations (hereafter referred as $\Delta G_{TC}$), for each $CO_2$ concentration. As expected, the frequency of TC genesis increases in the warm region and decreases in the cold region. The increase in genesis rate over warm regions is smaller than the decrease over cold regions but both positive and negative

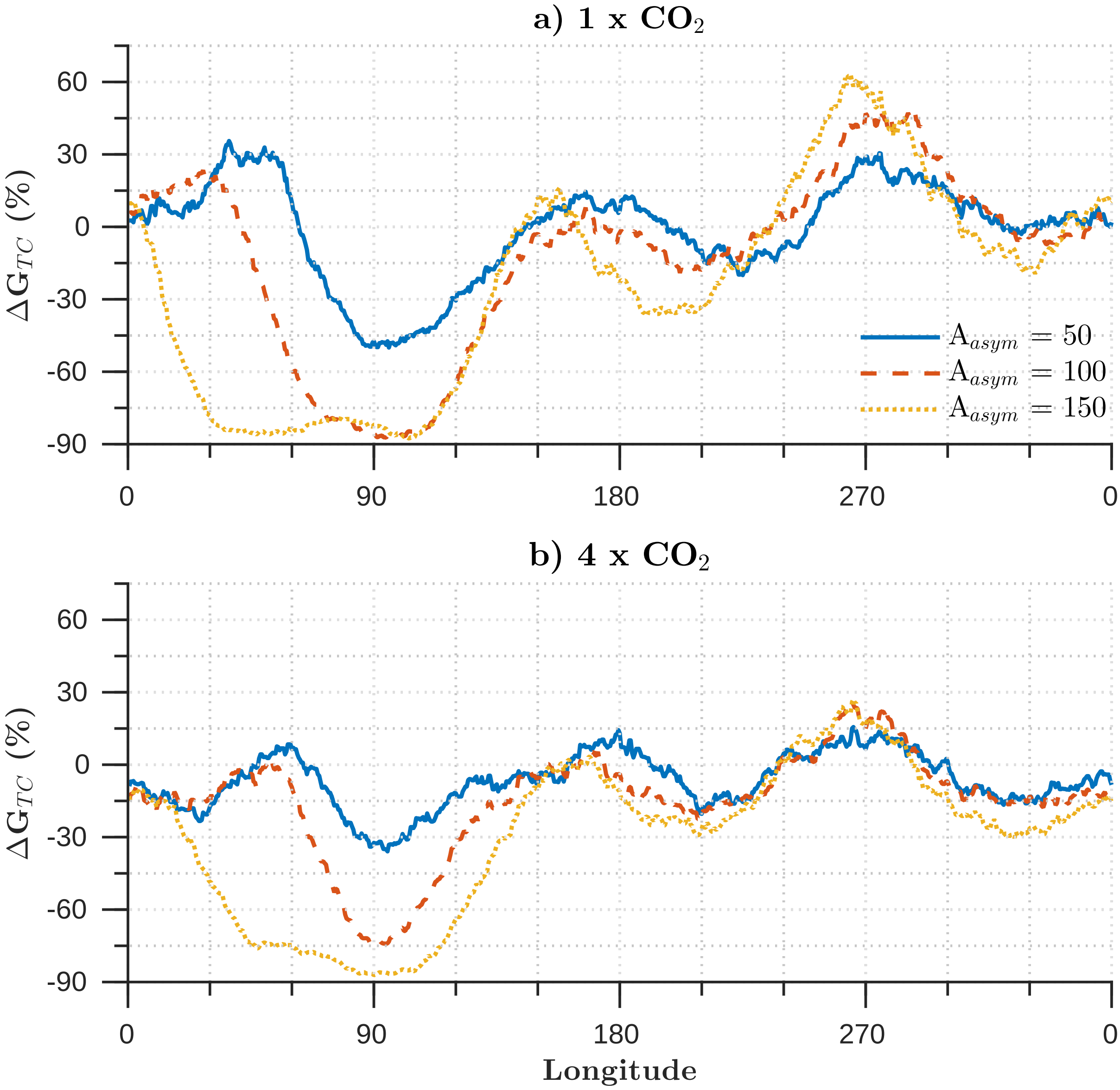


Figure 5–5: Relative changes in the rate of TC genesis ($\Delta G_{TC}$) with respect to zonally symmetric simulation vs longitude, for simulations with different magnitudes of the asymmetric part of the Q-flux ($A_{asym}$) and (a) 1 x $CO_2$ and (b) 4 x $CO_2$.

anomalies are larger than the natural level of variability (4.5%). There are also small reversed anomalies on either sides of the forcing regions, consistent with weak local SST and precipitation rate anomalies.

The asymmetry of the response in TC genesis is also amplifies if $A_{asym}$ increases. Moreover, increasing the $CO_2$ concentration damps the effect of asymmetry, especially over the warming region. In the cooling region near 90°E for the simulation with 1 x $CO_2$ and $A_{asym}$ = 150 W $m^2$, it seems that a minimum value for $\Delta G_{TC}$ is reached. This corresponds to an absolute value of TC genesis near zero (Fig. 5–4). Moreover, in this case the negative anomaly in the number of TCs expands westward and $\Delta G_{TC}$ is negative westward of the area of negative Q', whereas it is positive with weaker Q'. Therefore, we expect that if $A_{asym}$ is increased even more, the magnitude of $\Delta G_{TC}$ will not decrease more—$G_{TC}$ has zero as a lower bound—but the longitudinal extent of the negative area will continue to increase.

The profiles of the difference between asymmetric and symmetric conditions in the number of hurricanes are similar (not shown), with changes in the number of hurricanes over the warm region, near 270°E, that are greater than the relative changes in TC number.

Table 5–2 shows the globally averaged genesis rate for tropical cyclones and hurricanes (respectively $G_{TC}$ and $G_H$). It shows that the total number of tropical cyclones and hurricanes decreases when asymmetric conditions are prescribed, except the number of hurricanes in 1 x $CO_2$ simulations that varies non-monotonically as the asymmetry is increased. This suggests that zonally asymmetric Q-flux, which affects potential intensity, changes the TC intensity distribution, as indicated by the fraction of TCs that are hurricane strength in Table 5–2.

The larger the amplitude of the asymmetries, the smaller are the total numbers of TCs and hurricanes. This is consistent with the fact that the negative anomaly in $G_{TC}$ and $G_H$ is of bigger magnitude than the positive anomaly (Figure 5–5, such that the sum is negative. Even if zero is an lower bound of the number of storms, the westward expansion of the region of negative $\Delta G_{TC}$ observed for $A_{asym}$ = 150 W $m^2$ suggest that the total number of storms will keep decreasing if the amplitude of the asymmetry is increased.

The last rows of Table 5–2 shows the effect of quadrupling $CO_2$ on the total number of storms. The increase in the total TC and hurricanes numbers in 4 x $CO_2$ simulations with respect to the reference climate (1 x $CO_2$) has been attributed to the poleward shift of the ITCZ (*Merlis et al.*, 2013). While the number of hurricanes is more sensitive to quadrupling $CO_2$ concentration than TCs for statistically symmetric climates, this sensitivity decreases with $A_{asym}$. Indeed, with symmetric boundary conditions, quadrupling $CO_2$ leads to a 30% increase in $G_{TC}$ whereas $G_H$ increases by a factor of about 2.5. With asymmetric boundary conditions, this disparity in sensitivity to $CO_2$ concentration between TCs and hurricanes decreases to a 20% increase in $G_{TC}$ and a 80% increase in $G_H$.

The reduction of the sensitivity of TC genesis frequency to $CO_2$ concentration with increasing asymmetry seem to come from the asymmetric response between the cold and warm region (Figure 5–6). In 4 x $CO_2$ simulations, the genesis rate in the warm region is nearly insensitive to the amplitude of Q' (Figure 5–5. Therefore, the change in the total number of TCs with the amplitude of the zonally asymmetric Q-flux is almost exclusively due to the decrease in the cold region. In 1 x $CO_2$ simulations, the genesis rate in the warm region does change with the amplitude of Q' and counterbalances the decrease over the cold region. Therefore, the decrease of the global TC genesis rate in zonally asymmetric climate is stronger in 4 x $CO_2$ simulations than in 1 x $CO_2$ simulations. This explains the reduction of the difference between TC genesis frequency in 1 x $CO_2$ and 4 x $CO_2$ simulations.

## 5.5 Comparative influence of SST and latitude of ITCZ

Storm genesis is sensitive to both tropical-mean SST and latitude of ITCZ (*Merlis et al.*, 2013), with opposite effects. A poleward shift of ITCZ tends to increase the number of storms whereas an increase in SST tends to reduce it. This can be verified in these simulations comparing regions with similar latitude of ITCZ and different SST, and vice versa.

Table 5–2: Globally averaged genesis rate of tropical cyclones and hurricanes, given as the number of events per year, and fraction of TCs that reach hurricane strength ($f_H$), given as the number of events per year, in simulations with different amplitudes of the asymmetric energy flux ($A_{asym}$) and either 1 x $CO_2$ or 4 x $CO_2$, in # $yr^{-1}$. $\Delta_{150}$ is the percentage decrease in the total number of storms between the asymmetric simulation with $A_{asym}$ = 150 W $m^2$ and the symmetric one. $\Delta_{4xCO_2}$ is the relative increase in the number of storms due to quadrupling $CO_2$ concentration.

| $\mathbf{CO_2}$ | $\mathbf{A}_{asym}$ | $\mathbf{G}_{TC}$ | $\mathbf{G}_H$ | $\mathbf{f}_H$ |
|---|---|---|---|---|
| 300 | 0 | 343 | 26.4 | 7.69% |
| | 50 | 340 | 30.6 | 9.01% |
| | 100 | 304 | 30.9 | 10.2% |
| | 150 | 262 | 26.3 | 10% |
| | $\Delta_{150}$ | -23.6% | -0.379% | |
| 1200 | 0 | 448 | 69.8 | 15.6% |
| | 50 | 416 | 61.5 | 14.8% |
| | 100 | 380 | 60.2 | 15.8% |
| | 150 | 314 | 47.1 | 15% |
| | $\Delta_{150}$ | -30% | -32.5% | |
| $\Delta_{4xCO_2}$ | 0 | 30.5% | 164% | |
| | 50 | 22.6% | 101% | |
| | 100 | 25.1% | 94.8% | |
| | 150 | 19.7% | 79.1% | |

Comparing regions with the same latitude of ITCZ but different absolute SST confirms that warming tends to disfavor storm genesis (Figure 5–6). On the contrary, looking at two regions with similar SST but different latitudes of ITCZ shows that a poleward shift of ITCZ, at constant SST, favors storm genesis.

The fluctuations in the number of tropical cyclones and hurricanes seem to be less sensitive to the SST anomalies relative to the mean SST of the northern hemisphere main development region (6°N - 20°N). We examine the ITCZ latitude and the relative SST anomalies in three regions: the cold region (45°E - 135°E), the warm region (225°E - 315°E), and the neutral region (elsewhere), meridionally averaged between 4°N and 20°N. Figure 5–6 shows the genesis rates of tropical cyclones and hurricanes in these three regions for the six simulations (Table 5–1), versus ITCZ latitude and versus relative SST. The TC and hurricane frequencies increase with ITCZ latitude roughly linearly. However, there is no clear correlation between $G_{TC}$ and $G_H$ and the relative SST. Here we follow the averaging convention of taking the zonal mean over the latitudes where there is the most tropical cyclone activity as the mean SST (*Swanson*, 2008). However,

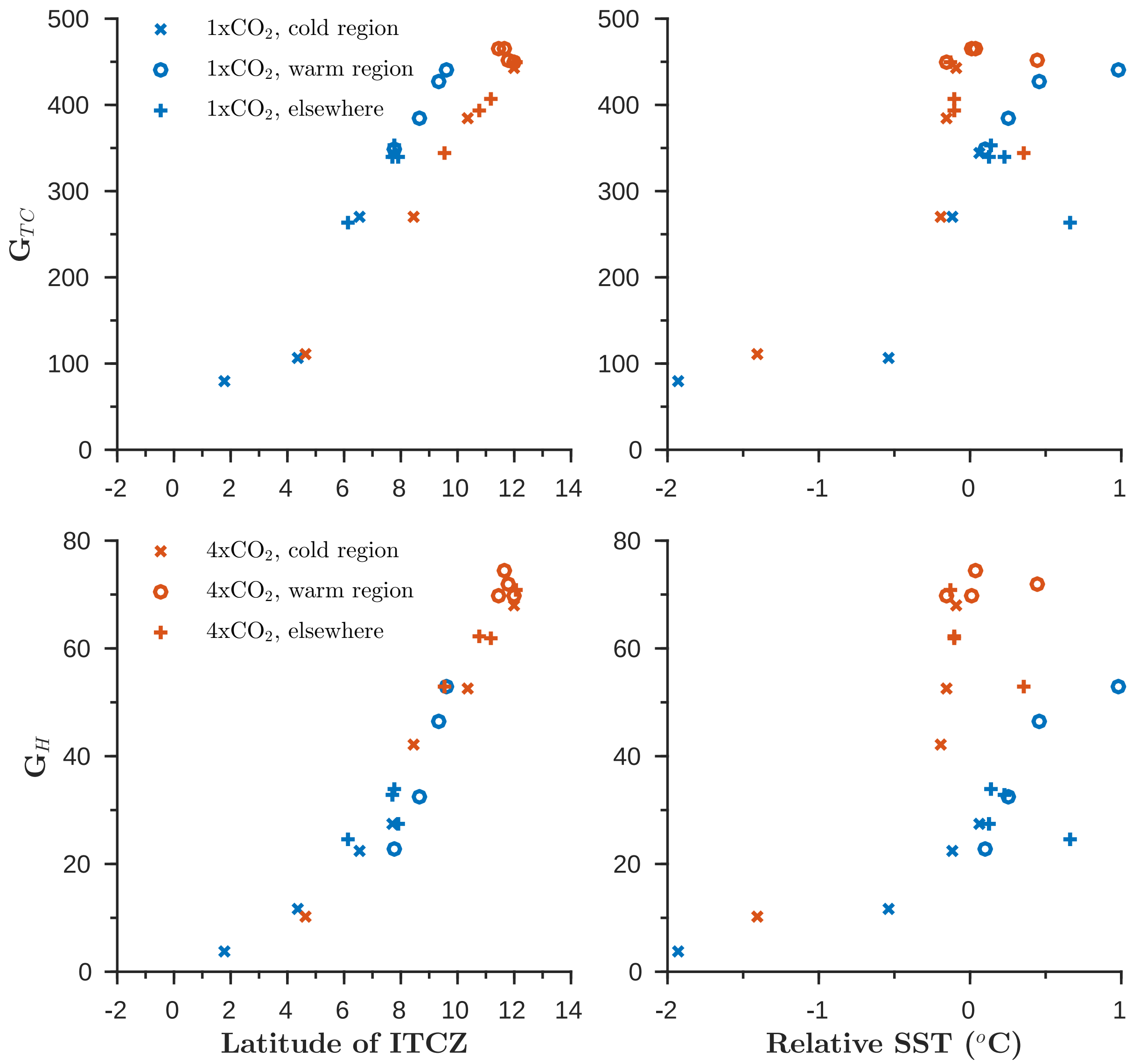


Figure 5–6: Genesis rates of tropical cyclones ($G_{TC}$, top panels) and hurricanes ($G_H$, bottom panels) (left) vs ITCZ latitude and (right) vs SST anomalies relative to the mean SST of the main development region (6°N - 20°N). The cold (45°E - 135°E), warm (225°E - 315°E), and neutral (elesewhere) regions are examined in the six different simulations (Table 5–1).

the correlation between relative SST and TC frequency is sensitive to the latitude used to define the mean SST. For instance, when the southern hemisphere tropics are included, the correlation is better, but there is no obvious justification to do so.

Consequently, the effect of ITCZ shift is competing against the impact of changes in absolute SST. In the simulations performed here, the effect of ITCZ shift seems predominant because in the warm (cold) region with more poleward (equatorward) ITCZ and warmer (colder) relative SST, the genesis rates of TCs and hurricanes increase (decrease).

## 5.6 Conclusions

Storm genesis and deep convection are sensitive to environmental conditions, such as SST patterns and ITCZ location. Adding the zonally asymmetric part of the energy flux changes the environmental conditions in and around the regions of forcing. In the region of positive Q-flux anomaly (60°E - 120°E ; 4°N - 20°N), the response is stronger than in the region of negative Q-flux anomaly (240°E - 300°E ; 4°N - 20°N). This dissimilarity of the responses may be explained by the sensitivity of planetary albedo on cloud amount.

SST is strongly correlated with energy fluxes such that SST pattern is similar to the prescribed field of Q-flux, though with opposite sign, with the negative response larger than the positive one. Deep convection is positively correlated to SST pattern and precipitation rate show anomalies of the same sign and same relative amplitude as SST anomalies, especially with a negative response stronger than the positive one. Another parameter that is perturbed by the prescription of zonally asymmetric conditions is the latitude of ITCZ. It shifts poleward in the warm region and equatorward in the cold region. In short, the larger is the amplitude of the zonally asymmetric part of the Q-flux, $A_{asym}$, the stronger are the response anomalies in SST, precipitation, and ITCZ meridional migration. Tropical cyclones and hurricanes show local genesis rates that increase in the region where the prescribed Q-flux is negative and decrease even more in the region where the prescribed flux is positive. The positive and negative anomalies in TC and hurricane genesis rates are significant, as they are larger than the level of "natural" variability. The dissimilarity between the positive and negative anomalies leads to a global decrease of tropical cyclones and hurricane frequencies when zonally asymmetric conditions are prescribed. As TC and hurricane genesis rate cannot decrease by more than 100%, when the $A_{asym}$ is large, the negative anomaly gets stronger by extending westward of the forcing region. Thereby, the negative anomaly stays greater than the positive one and the total number of hurricanes and tropical cyclones decreases in zonally asymmetric conditions.

Storm genesis is sensitive to both changes in SST and latitude position of the ITCZ, that have competing effects. In contrast, the relative SST—defined as the difference with the zonal mean SST—seem not to have a major influence on tropical cyclone frequency. The effect of ITCZ shift is dominant and explains the increase of TC and hurricane numbers in the warm region where the ITCZ shifts poleward. The frequencies of TCs and hurricanes are also sensitive to $CO_2$ concentration, even though this sensitivity decreases with the amplitude of the zonally asymmetric part of the Q-flux, because the absolute number of storms in the cold region near 90°E becomes very small.

In a context of climate change, it would be interesting to understand whether storm genesis is more sensitive to SST distribution or to the pattern of energy fluxes and this question could be addressed in subsequent work.

# CHAPTER 6
# General conclusion

Tropical cyclones are natural phenomena whose genesis mechanisms are not fully understood yet. Many environmental parameters, such as sea surface temperature, surface air moisture, and vertical wind shear are thought to influence tropical cyclogenesis. This study focused on sea surface temperature and examined its relationship with tropical cyclone genesis through three different aspects: the distribution of observed SSTs at time of genesis, observed long-term trends in SST at time of genesis, and the impact of SST regional pattern in GCM simulations.

The basin-by-basin analysis of the distribution of SST at tropical cyclone genesis shows that it is very similar to the distribution of SSTs observed in summer environment of the corresponding basin and differ between the basins. Over each basin the likelihood of tropical cyclone genesis increases with temperature until a certain SST, that is generally slightly colder than the basin mean, and the likelihood of genesis is insensitive to SST for warmer SSTs. The smooth increase of genesis likelihood with temperature and the differences between basins cast doubt about the concept of a global threshold SST for TC genesis.

The distributions of the vertical difference in equivalent potential temperature show more significant differences between the time of genesis and the summer environment, suggesting that this measure of convective instability is a better predictor for tropical cyclone genesis than SST.

The study of the time series of SST at TC genesis shows that it is highly correlated with those of SST observed in summer environment. The SST averaged over the location of all deep convection events also show similar mean values, year-to-year variations, and trends. These resemblances indicate that SST in and of itself is not a good predictor for TC genesis, as it does not allow to discriminate tropical cyclone from any other deep convection events. However, other parameters of tropical cyclone activity, such as TC rainfall and potential intensity, are influenced by SST, such that the newly observed trend in SST at TC genesis leads to expectations of changes in these parameters. Furthermore, the similarity in trends between SST at TC genesis and summer-season SSTs suggest that TCs can be used as indicators of reanalysis products and GCM accuracy.

The third part of this work examines how zonal asymmetries in Earth's climate influence tropical cyclone genesis. The region with prescribed divergent ocean energy flux (cold region) responds more strongly than the region where the ocean energy flux converges (warm region). The surface temperature, precipitation rate, and storm frequency in the former region decreases more than it increases in the latter. This asymmetry in the response likely comes from changes in cloud cover and results in a decrease of the storm frequency. Local changes in tropical cyclone and hurricane genesis rates are mostly due to local shifts of the ITCZ—poleward shift leading to an increase in storm frequency—slightly counterbalanced by the changes in local SST—increasing SST resulting in a decrease in storm frequency.

In conclusion, sea surface temperature at tropical cyclone genesis reflects mean SST in summer environment. Especially, its long-term trend reflects the climatological warming trend, which is suggestive of anthropogenic climate change. Observational support for the concept of threshold SST for tropical cyclone genesis is weak, especially on a global scale, and SST in and of itself is not a good predictor for tropical cyclone genesis. Regional changes in environmental parameters affect storm frequency, especially absolute and relative SST changes and shift in latitude of the ITCZ, which have opposite effects. In the different simulations performed here, the effect of absolute SST is minor compared to ITCZ shift, resulting in a global decrease of tropical cyclone frequency under zonally asymmetric conditions.

# APPENDIX A
## Supplementary information for "Distribution of sea surface temperature at tropical cyclone genesis across ocean basins"

### A.1 Method of bootstrapping for percentile values

The statistical samples studied here are quite small, so a method of bootstrapping is used to determine the confidence interval of the percentile values (*Efron and Tibshirani*, 1994).

The basic principle of bootstrapping is to create a large number B of samples of the same size than the initial distribution, using random sampling with replacement. For each of these B bootstrap samples, the value of the statistic of interest T is computed to obtain a sampling distribution of T. The 95% confidence interval for T corresponds to the $2.5^{th}$ and $97.5^{th}$ quantiles of the B replications of T.

In our study, the statistics of interest are the values of all the percentiles between 0.5% and 99.5%, every 0.5%. We obtained an estimation of the 95% confidence interval for these statistics using the bootstrapping method with B=10000. The values of the $SST_G$ percentiles obtained by interpolation on the initial distribution and the confidence intervals obtained with bootstrapping are used in Figure 1.

### A.2 Method of calculation of the vertical difference in equivalent potential temperature

The difference between upper- and lower-level equivalent potential temperature is a measure of the convective instability of atmosphere. The lower-level is taken near surface and the upper-level is set at 500 hPa. This choice is justified by Figure A–1 that shows the vertical profile of equivalent potential temperature at genesis for 20 TCs in each basin and the average over these 20 events (red). The 20 TCs examined here are selected such that the probability distribution of $SST_G$ for these 20 events corresponds to the $SST_G$ probability distribution of the corresponding basin.

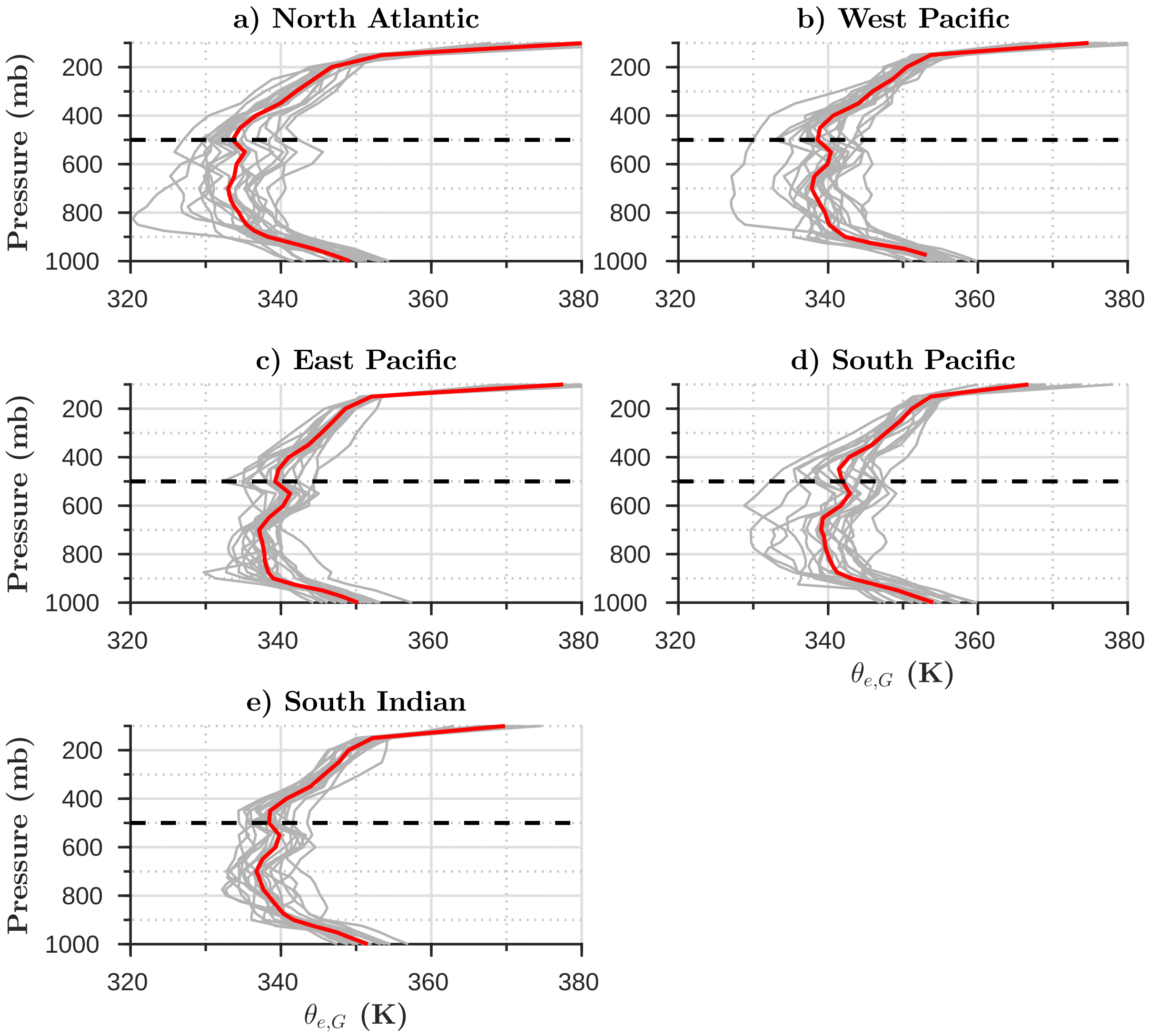


Figure A–1: Vertical profile of equivalent potential temperature averaged over the 3 days preceding genesis ($\theta_{e,G}$) for 20 TCs (thin grey lines) and the average over these events (red line) for each basin: a) North Atlantic basin, b) West Pacific basin, c) East Pacific basin, d) South Pacific basin, e) South Indian basin. The 500 hPa level is shown in dashed line.

Figure A–1 shows that, for all the basins, the 500 hPa level (dashed line) is a good approximation of the minimum in equivalent potential temperature in the upper-troposphere. Consequently, the difference between $\theta_{e,G}$ at 500 hPa and near surface generally reflects the convective instability of the atmosphere at TC genesis.

Figure A–2 shows the 20 days time-series of $\delta\theta_e$ at the location of genesis of 20 TCs in each basin, and the average over these 20 events. It can be seen that when the TC approaches, $\delta\theta_e$ increases, peaks the day of genesis (dashed-line) and then decreases. Consequently, the effect of the TC itself generally starts to be substantial 2 days before genesis. In order to examine the environmental condition and not probe the inflow layer of an existing storm, the values of equivalent potential temperature are averaged over the 3 days preceding genesis (day -3 to day -1) at the grid point corresponding to the genesis location.

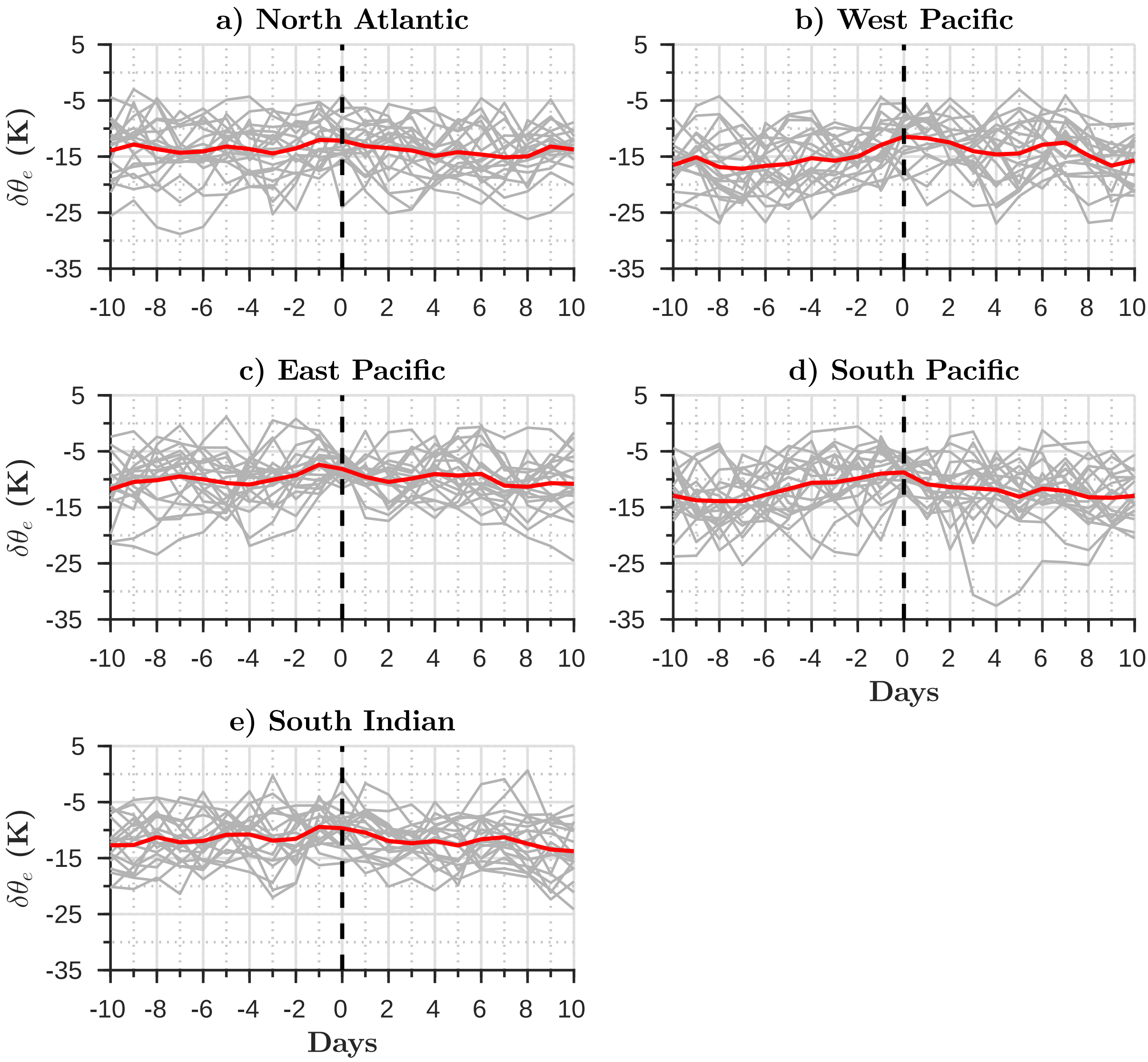


Figure A–2: Time-series of the difference in equivalent potential temperature between upper- and lower-level troposphere ($\delta\theta_e$) at the location of genesis of 20 TCs (thin grey lines) and the average over these events (red line) for each basin: a) North Atlantic basin, b) West Pacific basin, c) East Pacific basin, d) South Pacific basin, e) South Indian basin. The day of genesis is shown in dashed line and the time-series span 10 days before and 10 days after genesis.

# APPENDIX B
# Supplementary Information for "Observed trends in sea surface temperature at tropical cyclone genesis and for tropical deep convection"

## B.1 Sensitivity of SST at TC genesis to temporal resolution

Figure B–1 shows the time series of SST at TC genesis, obtained by linear interpolation from daily-mean values and monthly-mean values from NOAA/OISST data with two different spatial resolution. SSTs obtained from monthly means and/or with low spatial resolution (LR, brown) are generally warmer than those obtained with higher resolution temporal and/or spatial resolution. The two time series obtained with high spatial resolution data (daily and HR monthly-mean) show similar year-to-year variations and the same long-term trend of $0.18^o$ C per decade.

However, the differences between the two time series with the same monthly temporal resolution but different spatial resolution are substantial. The trend of $0.11^o$ C per decade obtained with the monthly-mean SSTs at low spatial resolution is close to the one observed in previous studies that use these temporal and spatial resolution*Flannaghan et al.* (2014); *Johnson and Xie* (2010).

This figure shows that SSTs at TC genesis are not sensitive to the temporal resolution of SST data set used for computation but that the two NOAA/OISST products with different spatial resolutions lead to different SST trends.

## B.2 SST trends with HadISST data set

Figure B–2 shows the time series of SST at TC genesis ($SST_G$), SST over the main development regions during TC season ($SST_S$), and SST during tropical deep convection events ($SST_{conv}$) obtained using SST values from HadISST data set. Using this data set of monthly-mean SSTs, the values obtained for $SST_G$, $SST_S$, and $SST_{conv}$ are globally warmer than those obtained with NOAA/OISST dataset. The warmer values are consistent with the sensitivity to the temporal resolution (Fig. B–1).

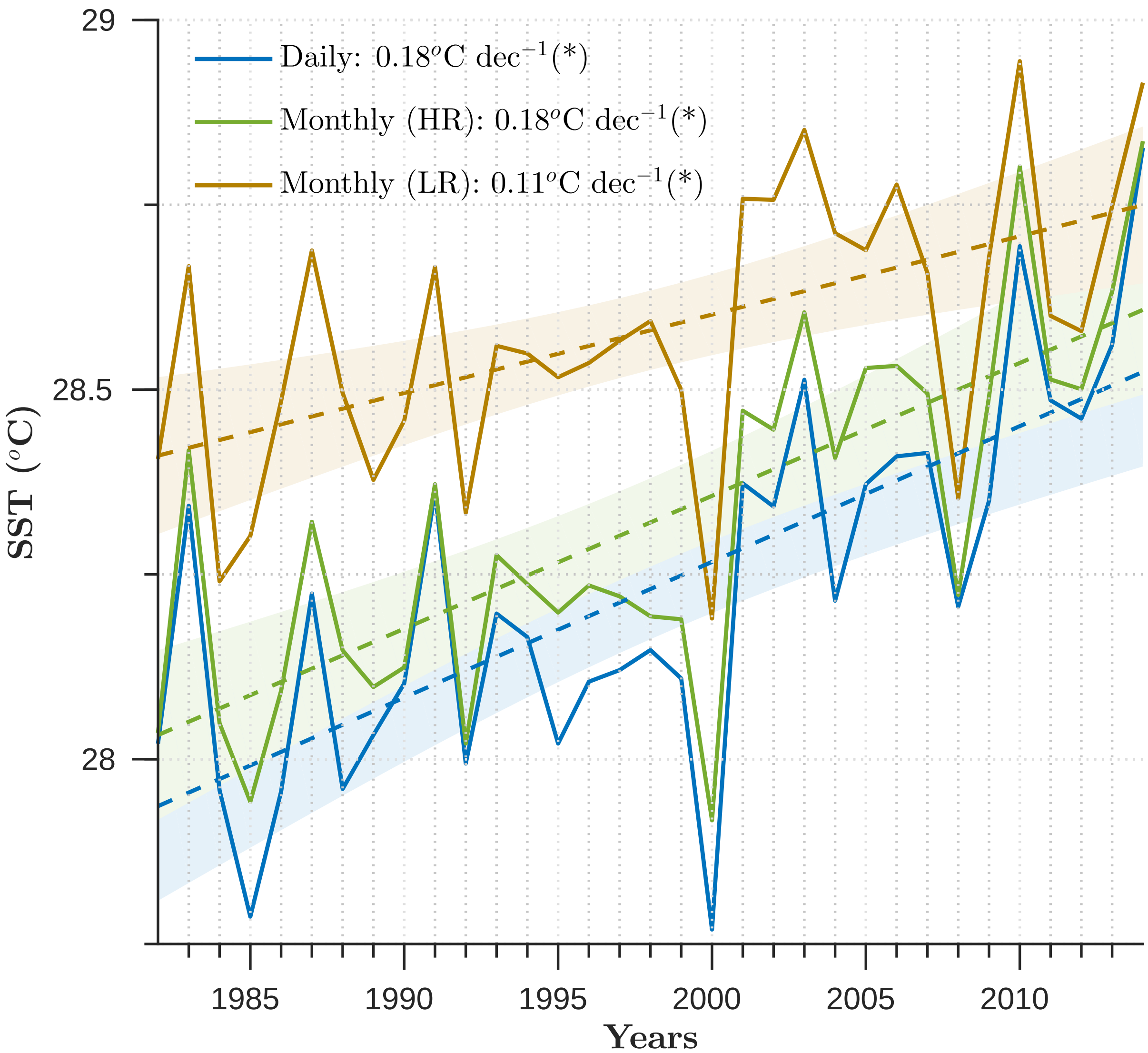


Figure B–1: Time series of SST at tropical cyclone genesis obtained using daily-mean values (blue) and monthly-mean values (green) of SST, from the NOAA/OISST with $0.25^o$ spatial resolution (high resolution, HR), and with daily-mean values from NOAA/OISST with $1^o$ resolution (low resolution (LR), brown). The three time series correspond to SSTs averaged over the 5 basins with the most TC activity.

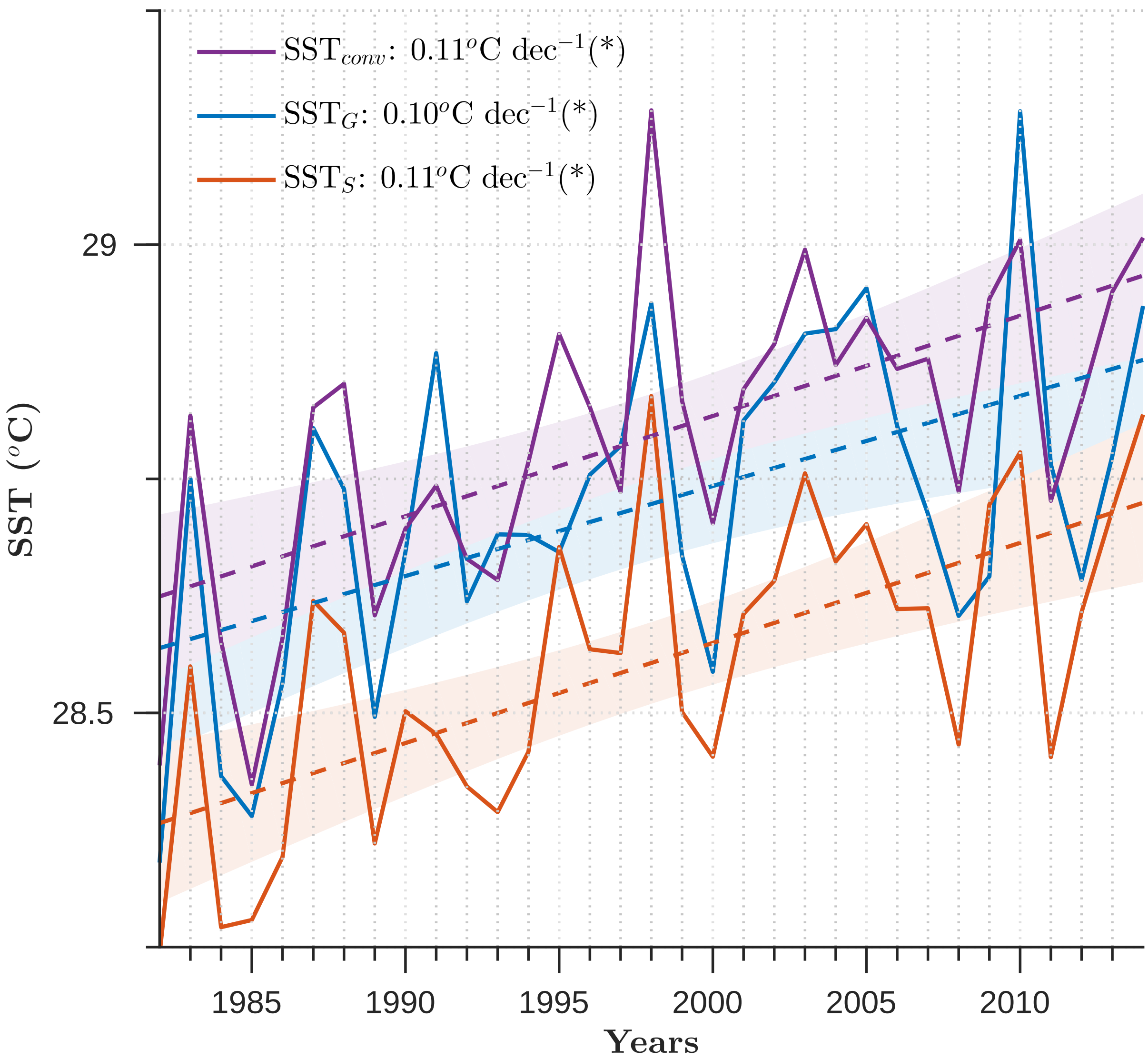


Figure B–2: Observed time series of SST$_G$, SST$_{conv}$, and SST$_S$ , averaged over the 5 basins with the most TC activity during TC season. SST at TC genesis (SST$_G$), SST at location of deep tropical convection (SST$_{conv}$) and SST over the main development regions during TC season (SST$_S$) are calculated using HadISST data between 1982 and 2014. For each curve the long-term linear trend (dashed lines) and the 95% confidence interval (shaded area) are also shown. The (*) indicates that the trend is statistically significant.

These three time series ($SST_G$, $SST_S$, $SST_{conv}$) are similar to each other within the HadISST dataset, though they differ significantly to those obtained with the NOAA/OISST data set. In particular, the long-term trends obtained with HadISST ($0.1^o$C dec$^{-1}$) are about half of the magnitude of the trends found using NOAA/OISST data ($0.2^o$C dec$^{-1}$). With both data sets, the long-term trends are significantly different from zero.

## B.3 Poleward migration of the location of tropical cyclone genesis

### B.3.1 Observed TC tracks

The global-mean latitude of the tropical cyclone life-time maximum intensity (LMI) has shifted poleward over the last 30 years at an approximate rate of $1^o$ per decade*Kossin et al.* (2014), which is similar to the observed rate of expansion of the width of the tropics*Johanson and Fu* (2009); *Archer and Caldeira* (2008); *Davis and Rosenlof* (2012). Here we compare the trend in latitude of TC genesis (i.e., the first time the maximum sustained wind speed reaches 18 m s$^{-1}$) and TC LMI. Figure B–3 shows the time series of the latitude of TC genesis and LMI observed between 1982 and 2014, using TC tracks from IBTrACS. The latter reproduces results from *Kossin et al.* (2014), except that only the TCs are considered in our study (i.e., storms with maximum sustained wind reaching at 18 m s$^{-1}$ at least once). The global-mean latitude of TC genesis has also shifted poleward over the last three decades according to IBTrACS, though at a somewhat smaller and not significant rate of approximately $0.81^o$ per decade. It suggests that the trend in LMI location is linked to the trend in genesis location. The smaller trend in the mean latitude of genesis compared to the mean latitude of LMI may arise from an increase in storm lifetime*Emanuel* (2005) or factors influencing TC intensification. The observed poleward migration of the location of tropical cyclone genesis and LMI are a sum of the intra-basin poleward shift of LMI and of the inter-basins variations due to the changes in the relative frequency of storms from each basin, where the contribution from intra-basin changes is dominant*Kossin et al.* (2014).

### B.3.2 Simulated TC tracks

The mean latitude of genesis for the TC tracks resulting from the CMIP5 AMIP HiRAM simulations are also examined. Figure B–4 shows the time series of latitude at

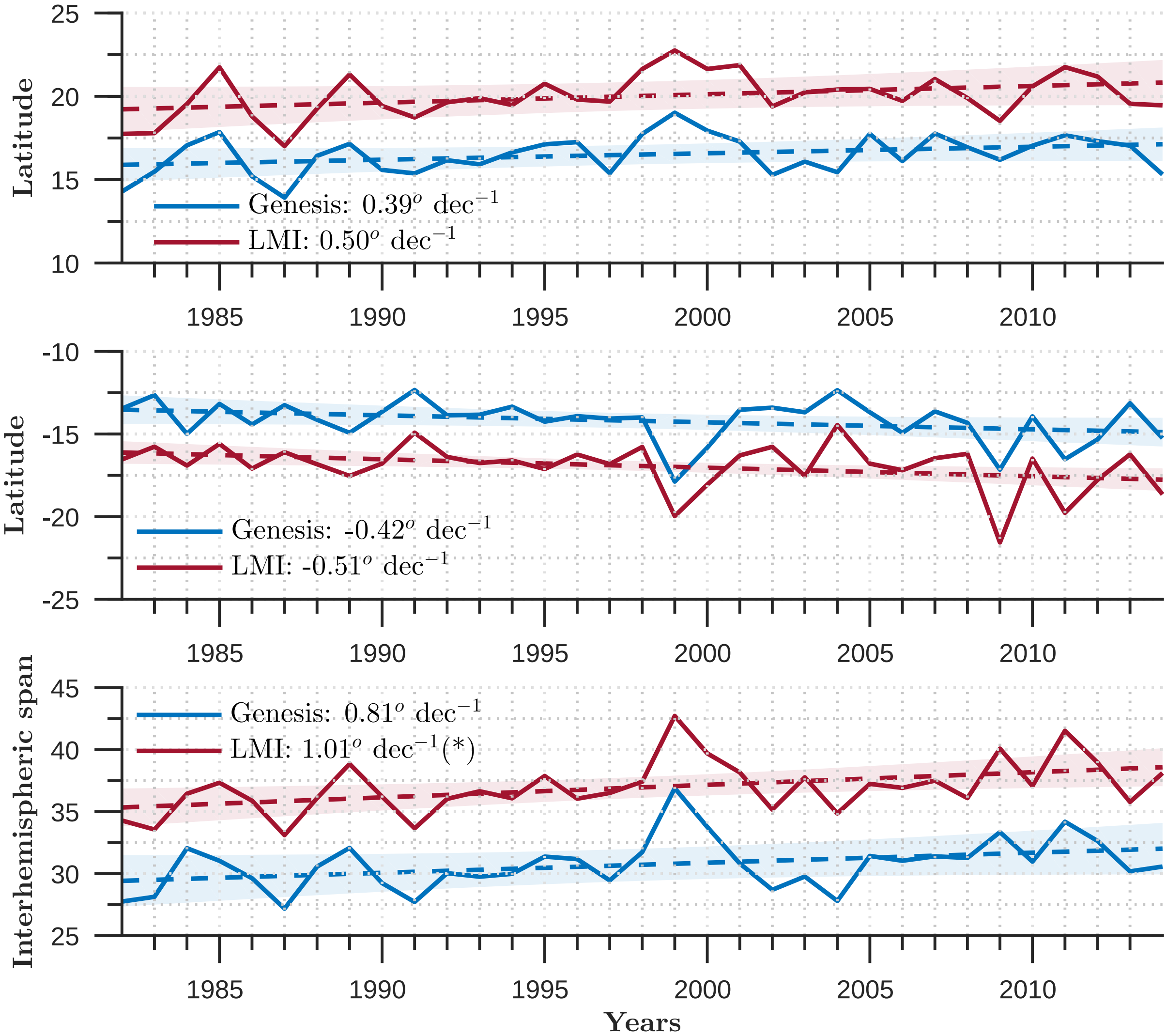


Figure B–3: Time series of latitude of tropical cyclone genesis (blue) and LMI (red) in the (a) Northern and (b) Southern hemispheres. (c) The difference between (a) and (b) gives an estimate of the global migration of the latitude of TC genesis and LMI away from the equator.

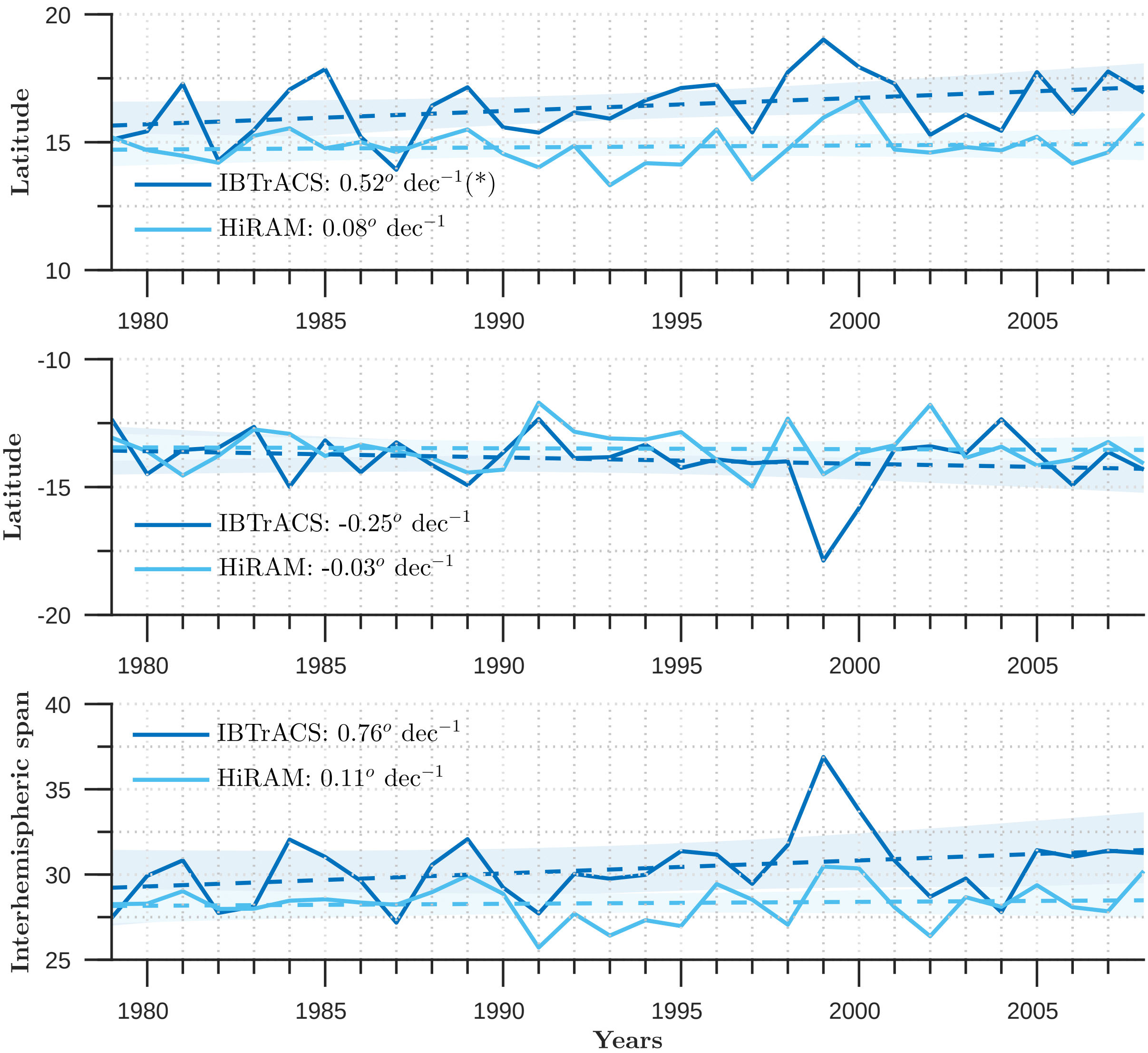


Figure B–4: Time series of latitude of tropical cyclone genesis observed (IBTrACS, dark blue) and simulated by HiRAM (light blue) in the (a) Northern and (b) Southern hemispheres. (c) The difference between (a) and (b) gives an estimate of the global migration of the latitude of TC genesis and LMI away from the equator.

TC genesis observed (IBTrACS) and simulated (HiRAM) between 1980 and 2008, and the corresponding long-term trends. Both time series show non-significant poleward trend and the simulated trend is much smaller than the observed one.

### B.4 Effect of ENSO on East Pacific SST trend

Figure B–5 shows the time series of SST at TC genesis and over the main development region during TC season for the East Pacific basin only. Figure B–5 also shows the time series of the Oceanic Niño Index (3 month running mean of NOAA's ERSST.v4 SST anomalies in the Niño 3.4 region ($5^o$N - $5^o$S, $120^o$ - $170^o$W)], based on centered 30-year base periods updated every 5 years.

It can be seen that there has been a La Niña-like decadal cooling, which is pronounced at the beginning of the $21^{st}$ century and may explain the absence of trend in East Pacific $SST_S$ (Table 1).

### B.5 Definition of main development regions and TC season

Table B–1: Spatial and temporal extent of the TC season for each basin. For the EP basin, the northwest area between $190^o$ - $239^o$E longitude and $16.5^o$ - $21^o$N latitude is excluded because there are few TC genesis events. Similarly, for the NA basin the northeast area between $325^o$E - $340^o$E and $18^o$N - $28^o$N is excluded. For the SI basin, the TC season of a given year includes the month of December of the preceding year.

| **Basin** | **Longitude** | **Latitude** | **TC season months** |
|---|---|---|---|
| NA | $263^o$ - $340^o$E | $10^o$ - $28^o$N | July to October |
| WP | $110^o$ - $170^o$E | $5^o$ - $25^o$N | June to November |
| EP | $190^o$ - $270^o$E | $8^o$ - $21^o$N | June to October |
| SP | $135^o$ - $220^o$E | $8^o$ - $20^o$S | January to April |
| SI | $40^o$ - $130^o$E | $5^o$ - $20^o$S | December to April |

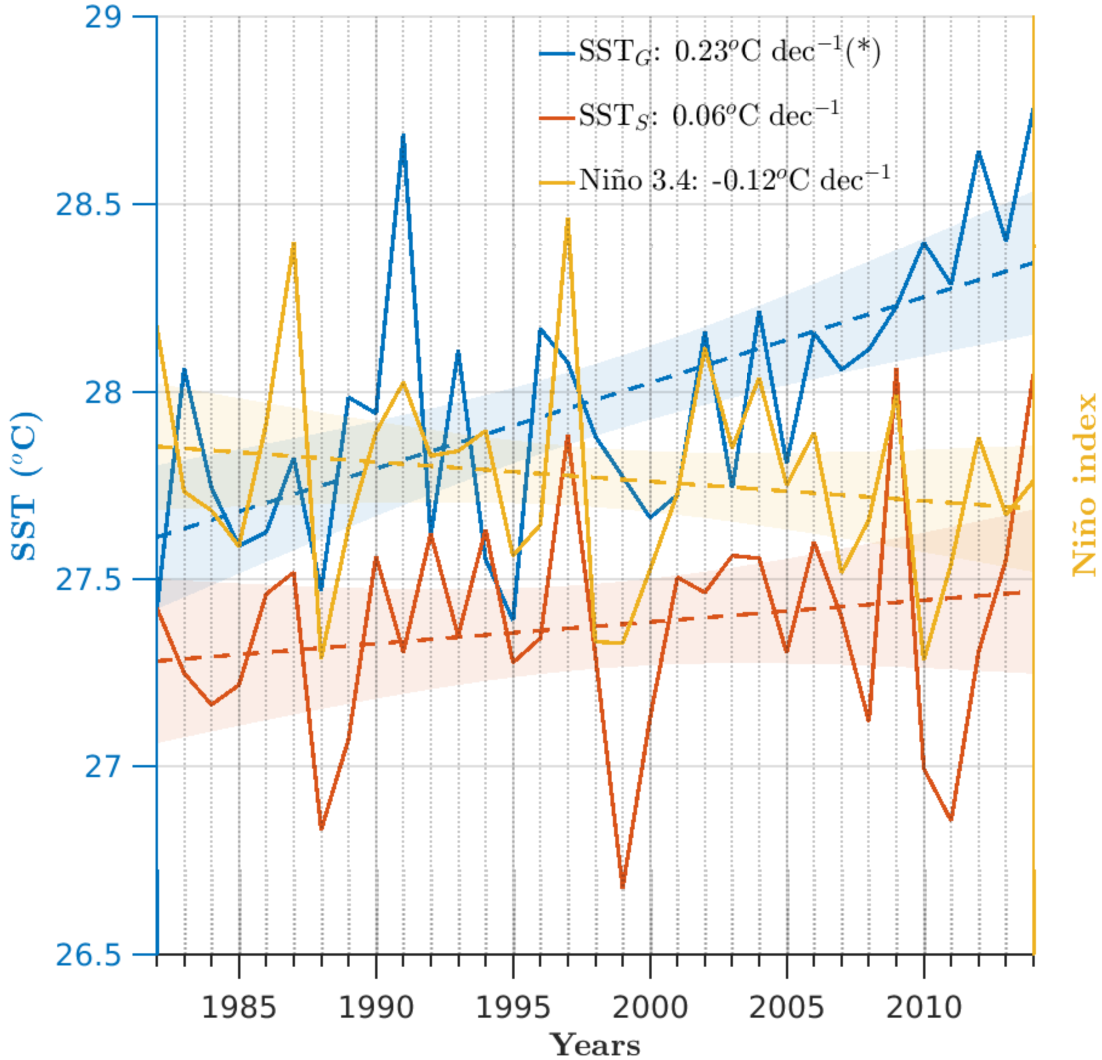


Figure B–5: Observed time series of $SST_G$ and $SST_S$, over the East Pacific basin, and Niño 3.4 seasonal SST index between 1982 and 2014. For each curve the long-term linear trend (dashed lines) and the 95% confidence interval (shaded area) are also shown. The (*) indicates that the trend is statistically significant.

# APPENDIX C
## Supplementary Information for "Response of tropical cyclone frequency to zonally asymmetric conditions in numerical simulations"

### C.1 Absolute values of environmental variables in zonally asymmetric simulations

Figure C–1 shows the absolute values of sea surface temperature, precipitation rate and latitude of the ITCZ, in response to zonally asymmetric prescribed Q-flux. We can see that all the variables are increased in response to $CO_2$ concentration increase.

### C.2 Profile of surface relative humidity in zonally asymmetric simulations

Figure C–2 shows the profile of surface relative humidity versus longitude, in response to zonally asymmetric prescribed Q-flux. The relative humidity increases to approximately 90% near 90°E, such that the temperature decrease needed to reduce the latent energy (LE) fluxes is greater in magnitude than it would be with the mean relative humidity (85%). In the region near 270°E, on the contrary, the relative humidity decreases slightly—which already acts to increase LE fluxes—such that the temperature response needed to increase more LE fluxes is muted.

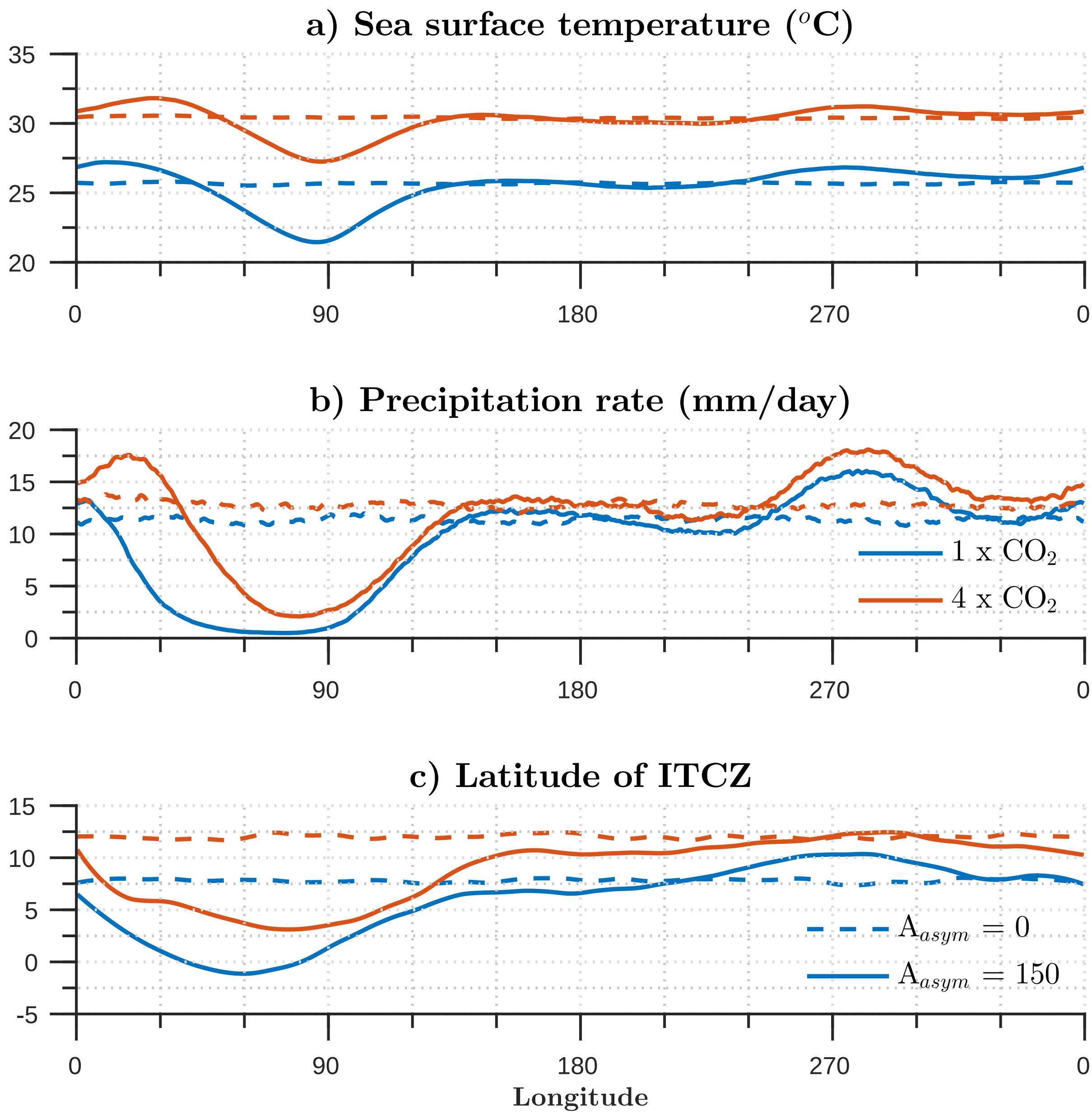


Figure C–1: Absolute values of (a) sea surface temperature, (b) precipitation and (c) the latitude of ITCZ, in zonally symmetric (dashed line) and asymmetric ($A_{asym}$= 150 W m$^{-2}$, solid line) simulations, for 1 x $CO_2$ and 4 x $CO_2$, in the region of forcing vs longitude. The variables are meridionally averaged between 4°N and 20°N.

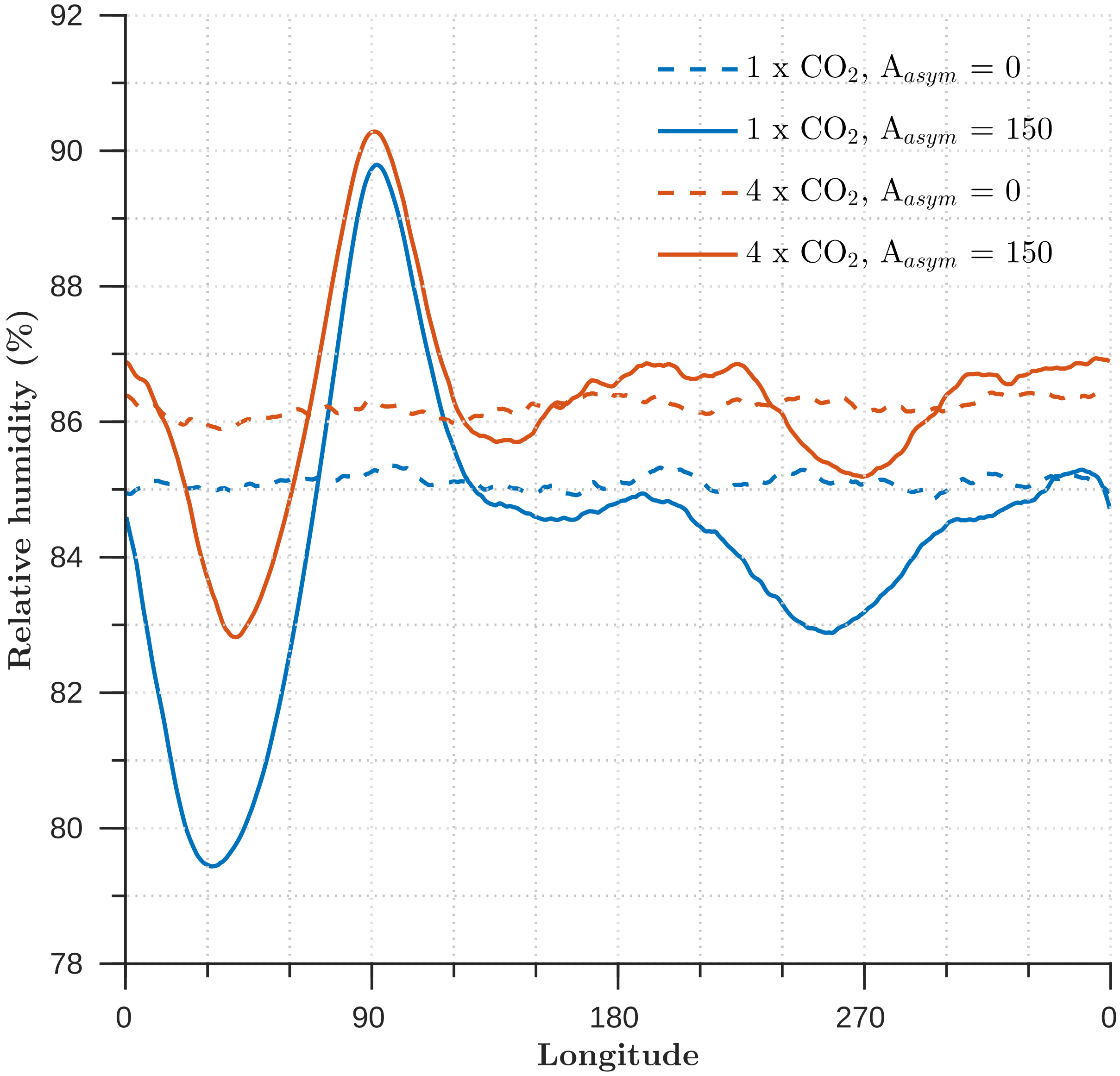


Figure C–2: Surface relative humidity vs longitude in zonally symmetric (dashed line) and asymmetric ($A_{asym}$= 150 W m$^{-2}$, solid line) simulations, for 1 x $CO_2$ (blue) and 4 x $CO_2$ (red), in the region of forcing vs longitude. The relative humidity is meridionally averaged between 4°N and 20°N.

REFERENCES


Archer, C. L., and K. Caldeira (2008), Historical trends in the jet streams, *Geophysical Research Letters*, *35*(8), n/a.

Bengtsson, L., K. I. Hodges, M. Esch, N. Keenlyside, L. Kornblueh, J.-J. Lou, and T. Yamagata (2007), How may tropical cyclones change in a warmer climate?, *Tellus*, *59A*, 539–561.

Berry, G., and M. J. Reeder (2014), Objective identification of the intertropical convergence zone: Climatology and trends from the ERA-Interim, *Journal of Climate*, *27*(5), 1894–1909.

Bhattacharyya, A. (1943), On a measure of divergence between two statistical populations defined by their probability distributions, *Bulletin of the Calcutta Mathematical Society*, *35*, 239–258.

Bolton, D. (1980), The Computation of Equivalent Potential Temperature, *Monthly Weather Review*, *108*(7), 1046–1053.

Camargo, S. J., A. H. Sobel, A. G. Barnston, and K. A. Emanuel (2007a), Tropical cyclone genesis potential index in climate models, *Tellus A*, *59*(4), 428–443.

Camargo, S. J., K. A. Emanuel, and A. H. Sobel (2007b), Use of a genesis potential index to diagnose ENSO effects on tropical cyclone genesis, *Journal of Climate*, *20*(19), 4819–4834.

Collins, M., R. Knutti, J. Arblaster, J.-L. Dufresne, T. Fichefet, P. Friedlingstein, X. Gao, W. J. Gutowski, T. Johns, G. Krinner, M. Shongwe, C. Tebaldi, A. J. Weaver, and M. Wehner (2013), Long-term Climate Change: Projections, Commitments and Irreversibility, in *Climate Change 2013: The Physical Science Basis. Contribution of Working Group I to the Fifth Assessment Report of the Intergovernmental Panel on Climate Change*, Cambridge University Press, Cambridge, United Kingdom and New York, NY, USA.

Dare, R. A., and J. L. McBride (2011), The threshold sea surface temperature condition for tropical cyclogenesis, *Journal of Climate*, *24* (17), 4570–4576.

Davis, S. M., and K. H. Rosenlof (2012), A multidiagnostic intercomparison of tropical-width time series using reanalyses and satellite observations, *Journal of Climate*, *25* (4), 1061–1078.

Efron, B., and R. J. Tibshirani (1994), *An introduction to the bootstrap*, CRC press.

Emanuel, K. (2003), Tropical cyclones, *Annual Review of Earth and Planetary Sciences*, *31* (1), 75–104.

Emanuel, K. (2005), Increasing destructiveness of tropical cyclones over the past 30 years, *Nature*, *436* (7051), 686–688.

Emanuel, K., and A. Sobel (2013), Response of tropical sea surface temperature, precipitation, and tropical cyclone-related variables to changes in global and local forcing, *Journal of Advances in Modeling Earth Systems*, *5* (2), 447–458.

Emanuel, K., R. Sundararajan, and J. Williams (2008), Hurricanes and Global Warming: Results from Downscaling IPCC AR4 Simulations, *Bull. Am. Meteor. Soc.*, *89*, 347–367.

Emanuel, K. A. (1987), The dependence of hurricane intensity on climate, *Nature*, *326* (6112), 483–485.

Emanuel, K. A. (1995), Sensitivity of Tropical Cyclones to Surface Exchange Coefficients and a Revised Steady-State Model incorporating Eye Dynamics, *Journal of the Atmospheric Sciences*, *52* (22), 3969–3976, doi:10.1175/1520-0469(1995)052¡3969:SOTCTS¿2.0.CO;2.

Emanuel, K. A. (2013), Downscaling CMIP5 climate models shows increased tropical cyclone activity over the 21st century, *Proc. Nat. Acad. Sci.*, *110*, 12,219–12,224.

Emanuel, K. A., and D. S. Nolan (2004), Tropical cyclone activity and the global climate system, in *Preprints, 26th Conf. on Hurricanes and Tropical Meteorology, Miami, FL, Amer. Meteor. Soc. A*, vol. 10.

Flannaghan, T. J., S. Fueglistaler, I. M. Held, S. Po-Chedley, B. Wyman, and M. Zhao (2014), Tropical temperature trends in Atmospheric General Circulation Model simulations and the impact of uncertainties in observed SSTs, *J. Geophys. Res. Atmos*, *119*, 13–327.

Graham, N. E., and T. P. Barnett (1987), Sea surface temperature, surface wind divergence, and convection over tropical oceans, *Science*, *238*(4827), 657–659.

Gray, W. M. (1968), Global view of the origin of tropical disturbances and storms, *Monthly Weather Review*, *96*(10), 669–700.

Held, I. M., and B. J. Soden (2006), Robust responses of the hydrological cycle to global warming, *Journal of Climate*, *19*(21), 5686–5699.

Held, I. M., and M. Zhao (2011), The response of tropical cyclone statistics to an increase in $CO_2$ with fixed sea surface temperatures, *Journal of Climate*, *24*, 5353–5364.

Holland, G. J. (1997), The Maximum Potential Intensity of Tropical Cyclones, *Journal of the Atmospheric Sciences*, *54*(21), 2519–2541, doi:10.1175/1520-0469(1997)054¡2519:TMPIOT¿2.0.CO;2.

Johanson, C. M., and Q. Fu (2009), Hadley cell widening: Model simulations versus observations, *Journal of Climate*, *22*(10), 2713–2725.

Johnson, N. C., and S.-P. Xie (2010), Changes in the sea surface temperature threshold for tropical convection, *Nature Geoscience*, *3*(12), 842–845.

Kang, S. M., and I. M. Held (2012), Tropical precipitation, SSTs and the surface energy budget: a zonally symmetric perspective, *Climate dynamics*, *38*(9-10), 1917–1924.

Kang, S. M., I. M. Held, D. M. W. Frierson, and M. Zhao (2008), The response of the ITCZ to extratropical thermal forcing: Idealized slab-ocean experiments with a GCM, *Journal of Climate*, *21*(14), 3521–3532.

Kang, S. M., D. M. W. Frierson, and I. M. Held (2009), The Tropical Response to Extratropical Thermal Forcing in an Idealized GCM: The Importance of Radiative Feedbacks and Convective Parameterization, *Journal of the Atmospheric Sciences*, *66*(9), 2812–2827, doi:10.1175/2009JAS2924.1.

Kirtman, B., S. B. Power, J. A. Adedoyin, G. J. Boer, R. Bojariu, I. Camilloni, F. J. Doblas-Reyes, A. M. Fiore, M. Kimoto, G. A. Meehl, M. Prather, A. Sarr, C. Schär, R. Sutton, G. J. van Oldenborgh, G. Vecchi, and H. J. Wang (2013), Near-term Climate Change: Projections and Predictability, in *Climate Change 2013: The Physical Science Basis. Contribution of Working Group I to the Fifth Assessment Report of the Intergovernmental Panel on Climate Change*, Cambridge University Press Cambridge, UK, and New York.

Knapp, K. R., M. C. Kruk, D. H. Levinson, H. J. Diamond, and C. J. Neumann (2010), The international best track archive for climate stewardship (IBTrACS) unifying tropical cyclone data, *Bulletin of the American Meteorological Society*, *91*(3), 363–376.

Knutson, T. R., J. L. McBride, J. Chan, K. Emanuel, G. Holland, C. Landsea, I. Held, J. P. Kossin, A. K. Srivastava, and M. Sugi (2010), Tropical cyclones and climate change, *Nature Geoscience*, *3*(3), 157–163.

Knutson, T. R., F. Zeng, and A. T. Wittenberg (2013), Multimodel assessment of regional surface temperature trends: CMIP3 and CMIP5 twentieth-century simulations, *Journal of Climate*, *26*(22), 8709–8743.

Kossin, J. P. (2015), Validating atmospheric reanalysis data using tropical cyclones as thermometers, *Bulletin of the American Meteorological Society*, *96*(7), 1089–1096.

Kossin, J. P., K. A. Emanuel, and G. A. Vecchi (2014), The poleward migration of the location of tropical cyclone maximum intensity, *Nature*, *509*, 349–352, doi: 10.1038/nature13278.

Lee, H. T. (2014), Climate Algorithm Theoretical Basis Document (C-ATBD): Outgoing longwave radiation (OLR) Daily. NOAA's Climate Data Record (CDR) program, CDRP-ATBD-0526, 46pp, *Tech. rep.*

McTaggart-Cowan, R., G. D. Deane, L. F. Bosart, C. A. Davis, and T. J. Galarneau Jr (2008), Climatology of tropical cyclogenesis in the North Atlantic (1948-2004), *Monthly Weather Review*, *136*(4), 1284–1304.

McTaggart-Cowan, R., E. L. Davies, J. G. Fairman Jr, T. J. Galarneau Jr, and D. M. Schultz (2015), Revisiting the 26.5$^o$C Sea Surface Temperature Threshold for Tropical

Cyclone Development, *Bulletin of the American Meteorological Society*, *96*(11), 1929–1943.

Merlis, T. M., and T. Schneider (2011), Changes in zonal surface temperature gradients and Walker circulations in a wide range of climates, *Journal of Climate*, *24*(17), 4757–4768, doi:10.1175/2011JCLI4042.1.

Merlis, T. M., M. Zhao, and I. M. Held (2013), The sensitivity of hurricane frequency to ITCZ changes and radiatively forced warming in aquaplanet simulations, *Geophysical Research Letters*, *40*(15), 4109–4114.

Merlis, T. M., W. Zhou, I. M. Held, and M. Zhao (2016), Surface temperature dependence of tropical cyclone-permitting simulations in a spherical model with uniform thermal forcing, *Geophys. Res. Lett.*, p. in press.

Nolan, D. S., and M. G. McGauley (2012), Tropical cyclogenesis in wind shear: Climatological relationships and physical processes.

Pachauri, R. K., M. R. Allen, V. R. Barros, J. Broome, W. Cramer, R. Christ, J. A. Church, L. Clarke, Q. Dahe, and P. Dasgupta (2014), Climate Change 2014: Synthesis Report. Contribution of Working Groups I, II and III to the Fifth Assessment Report of the Intergovernmental Panel on Climate Change.

Palmen, E. (1948), On the formation and structure of tropical hurricanes, *Geophysica*, *3*(1), 26–38.

Payne, B., and J. Methven (2012), The role of baroclinic waves in the initiation of tropical cyclones across the southern Indian Ocean, *Atmospheric Science Letters*, *13*(2), 88–94.

Rayner, N. A., D. E. Parker, E. B. Horton, C. K. Folland, L. V. Alexander, D. P. Rowell, E. C. Kent, and A. Kaplan (2003), Global analyses of sea surface temperature, sea ice, and night marine air temperature since the late nineteenth century, *Journal of Geophysical Research: Atmospheres*, *108*(D14).

Reynolds, R. W., T. M. Smith, C. Liu, D. B. Chelton, K. S. Casey, and M. G. Schlax (2007), Daily high-resolution-blended analyses for sea surface temperature, *Journal of Climate*, *20*(22), 5473–5496.

Rienecker, M. M., M. J. Suarez, R. Gelaro, R. Todling, J. Bacmeister, E. Liu, M. G. Bosilovich, S. D. Schubert, L. Takacs, and G.-K. Kim (2011), MERRA: NASA's modern-era retrospective analysis for research and applications, *Journal of Climate*, *24* (14), 3624–3648.

Santer, B. D., T. M. L. Wigley, J. S. Boyle, D. J. Gaffen, J. J. Hnilo, D. Nychka, D. E. Parker, and K. E. Taylor (2000), Statistical significance of trends and trend differences in layer-average atmospheric temperature time series, *Journal of Geophysical Research: Atmospheres*, *105* (D6), 7337–7356.

Santer, B. D., T. M. L. Wigley, P. J. Gleckler, C. Bonfils, M. F. Wehner, K. AchutaRao, T. P. Barnett, J. S. Boyle, W. Brüggemann, and M. Fiorino (2006), Forced and unforced ocean temperature changes in Atlantic and Pacific tropical cyclogenesis regions, *Proceedings of the National Academy of Sciences*, *103* (38), 13,905–13,910.

Schreck, C. J., J. Molinari, and A. Aiyyer (2011), A Global View of Equatorial Waves and Tropical Cyclogenesis, *Monthly Weather Review*, *140* (3), 774–788, doi:10.1175/MWR-D-11-00110.1.

Scott, D. W. (2010), Averaged shifted histogram, *Wiley Interdisciplinary Reviews: Computational Statistics*, *2* (2), 160–164.

Shaevitz, D. A., S. J. Camargo, A. H. Sobel, J. A. Jonas, D. Kim, A. Kumar, T. E. LaRow, Y. Lim, H. Murakami, and K. A. Reed (2014), Characteristics of tropical cyclones in high-resolution models in the present climate, *Journal of Advances in Modeling Earth Systems*, *6* (4), 1154–1172.

Shaw, T. A., A. Voigt, S. M. Kang, and J. Seo (2015), Response of the intertropical convergence zone to zonally asymmetric subtropical surface forcings, *Geophysical Research Letters*, *42* (22), 9961–9969.

Sobel, A. H. (2007), Simple models of ensemble-averaged precipitation and surface wind, given the sea surface temperature, *The Global Circulation of the Atmosphere, edited by T. Schneider and AH Sobel*, pp. 219–251.

Sobel, A. H., and S. J. Camargo (2011), Projected future seasonal changes in tropical summer climate, *Journal of Climate*, *24* (2), 473–487.

Sobel, A. H., I. M. Held, and C. S. Bretherton (2002), The ENSO signal in tropical tropospheric temperature, *Journal of climate*, *15*(18), 2702–2706.

Stocker, T. F. (2014), *Climate change 2013: the physical science basis: Working Group I contribution to the Fifth assessment report of the Intergovernmental Panel on Climate Change*, Cambridge University Press.

Sugi, M., H. Murakami, and J. Yoshimura (2009), A reduction in global tropical cyclone frequency due to global warming, *SOLA*, *5*, 164–167.

Swanson, K. L. (2008), Nonlocality of Atlantic tropical cyclone intensities, *Geochemistry, Geophysics, Geosystems*, *9*(4).

Tippett, M. K., S. J. Camargo, and A. H. Sobel (2011), A Poisson regression index for tropical cyclone genesis and the role of large-scale vorticity in genesis, *Journal of Climate*, *24*(9), 2335–2357.

Tory, K. J., and R. A. Dare (2015), Sea Surface Temperature Thresholds for Tropical Cyclone Formation, *Journal of Climate*, *28*(20), 8171–8183.

Trenberth, K. E., C. A. Davis, and J. Fasullo (2007), Water and energy budgets of hurricanes: Case studies of Ivan and Katrina, *Journal of Geophysical Research: Atmospheres*, *112*(D23).

Vecchi, G. A., K. L. Swanson, and B. J. Soden (2008), Whither hurricane activity, *Science*, *322*(5902), 687–689.

Vecchi, G. A., S. Fueglistaler, I. M. Held, T. R. Knutson, and M. Zhao (2013), Impacts of atmospheric temperature trends on tropical cyclone activity, *Journal of Climate*, *26*(11), 3877–3891.

Walsh, K. J. E., M. Fiorino, C. W. Landsea, and K. L. McInnes (2007), Objectively determined resolution-dependent threshold criteria for the detection of tropical cyclones in climate models and reanalyses, *Journal of climate*, *20*(10), 2307–2314.

Wing, A. A., K. Emanuel, and S. Solomon (2015), On the factors affecting trends and variability in tropical cyclone potential intensity, *Geophysical Research Letters*, *42*(20), 8669–8677.

Zhang, C. (1993), Large-scale variability of atmospheric deep convection in relation to sea surface temperature in the tropics, *Journal of Climate*, *6*(10), 1898–1913.

Zhao, M., and Others (2013), Robust direct effect of increasing atmospheric $CO_2$ concentration on global tropical cyclone frequency: A multimodel inter-comparison., *US CLIVAR Variations*, *11*, 17–24.

Zhao, M., I. M. Held, S.-J. Lin, and G. A. Vecchi (2009), Simulations of global hurricane climatology, interannual variability, and response to global warming using a 50-km resolution GCM, *Journal of Climate*, *22*(24), 6653–6678.